

Facultad de Ciencias –
Universidad de la
Laguna.

Master in Molecular
Nanoscience and
Nanotechnology

Course 2020-2021

Materials based on metal organic frameworks for the removal of emerging pollutants in water

Yaiza Martín García

Supervisor: Ana Belén Lago Blanco

Laboratorio de Materiales para Análisis Químicos (MAT4LL), Departamento de Química, Unidad Departamental de Química Inorgánica, Universidad de La Laguna (ULL), La Laguna, Tenerife, 38206, Spain.

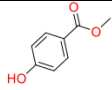
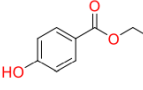
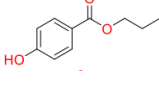
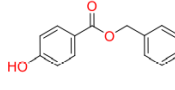
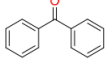
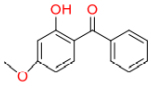
Photocatalysis and adsorption processes are used to achieve selective decomposition to produce clean water. New hybrid materials that incorporated selective oxidation and solid adsorption properties were used to achieve synergistic effects. Here, we propose the integration of metal-organic frameworks (MOFs) compounds with good adsorption properties with traditional photocatalytic materials to obtain new hybrid composite materials that absorb and catalyze various molecules of emerging pollutants. Different synthesis strategies were followed to integrate photocatalyst compounds and MOFs sorbents in the new composite materials. The synthesized composites were characterized by different techniques such as X-ray diffraction (XRD), thermogravimetric analysis (TGA), infrared spectroscopy (IR), dynamic light scattering (DLS) and N₂ adsorption experiments. The structural and extraction properties of these compounds were studied to obtain a detailed knowledge of the differences between the different composites.

Introduction

Water control has always been a topic of interest to get drinking water and avoid possible environmental and human health problems. Non-polar hazardous compounds (persistent organic pollutants (POPs) and heavy metals) are less relevant compounds since their emission has been controlled and the dominant sources of pollution have been eliminated.^[1]

However, the so-called unregulated emerging pollutants are synthetic or naturally occurring chemicals that have the potential to enter the environment and cause known or unknown adverse effects on human and / or ecological health, they are not controlled and do not exist enough information about them for their regulation.^[2] These environmental pollutants include disinfection by-product, drug of abuse, flame retardants, hormones, inorganic, and organic nanomaterials, microplastics, perfluorinated substances, pharmaceuticals, and personal care products, among others.^[3] In this work, we have focused our studies on the analysis of personal care products (PCPs), which include not only prescription and biological drugs, but also fragrances, sunscreen agents, among many others. These are a small but constant source of contamination in treated and untreated wastewater, which is a big problem since it leads to its progressive accumulation causing irreversible effects.^[4] In particular, we will use the PCPs preservative products listed in Table 1 together with the chemical structure and water solubility: methylparaben (MPB), ethylparaben (EPB), propylparaben (PPB), and benzylparaben (BzPB) and UV-filters called: benzophenone (BP) and 3-Benzophenone (3-BP).

Table 1. Name, structure, and water solubility of the different analytes

Analyte (abbreviation)	Structure	Water solubility (g/L) (25°C)
Methylparaben (MPB)		2.5
Ethylparaben (EPB)		2.5
Propylparaben (PPB)		2.5
Benzylparaben (BzPB)		2.5
Benzophenone (BP)		Insoluble
3-Benzophenone (3-BP)		Insoluble

In the last two decades, the use of metal-organic frameworks (MOFs) has increased as promising hybrid materials for gas sorption^[5], catalysis^[6], separation^[7] or wastewater treatment^[8], among others. MOFs are three-dimensional coordination polymers that can use a

wide variety of metal ions and organic ligands.^[9] MOFs can be used for size / shape-based separations due to the uniform pore size distribution and ordered pore structure. Furthermore, the versatility of organic linkers and metal ions used in MOFs introduces different types of interactions with analytes.^{[10][11]}

UiO-66 is a zirconium - based MOF built up from hexamers of eight coordinated $ZrO_6(OH)_2$ polyhedral and terephthalate ligands. In addition to its unique porous structure, UiO-66 also exhibits excellent chemical resistance to solvents such as water, benzene, dimethylformamide (DMF), and acetone.^[10] Several studies have already demonstrated the viability of functionalizing the UiO-66 material, without losing the physicochemical properties, and its advantages in the capture and separation of gases have been mainly analyzed^{[11][12][13]}. This functionalization of the linker establishes stronger host-guest interactions^[14] but implies a decrease in surface areas and pore volumes^[15].

The CIM-80 material (aluminium (III)-mesaconate based compound) has been synthesized in high yield through a green procedure involving water and urea as co-reactants with good thermal and water stability.^[16] The crystal lattice of CIM-80 (Al) is made up of octahedral structures of AlO_6 that interconnect through -OH groups and mesaconate molecules, giving rise to the formation of two different types of pores: one hexagonal and the other trigonal.

A composite is a material formed by the combination of two or more elements so that they are stronger as a whole than individually. We will focus our efforts on the formation of composites using different MOFs and a photocatalyst compound as precursors with the aim of obtaining core-shell structures, that is, where one of the materials is surrounded by the other.

Chromatographic separation is essential for the correct identification and quantification of the studied analytes. Liquid chromatography (LC) is based on the partition of the analytes between a liquid mobile phase and a solid stationary phase. It is the most widely used separation technique because of its versatility and sensitivity.^[17]

Photocatalysis is defined as the acceleration of a chemical reaction by the action of a solid catalyst, activated by electronic excitation when light radiation of a certain energy content falls on it.^[18]

Heterogeneous photocatalysis includes a great variety of reactions: mild or total oxidations, hydrogen transfer, water decontamination, removal of gaseous pollutants, etc.^[19]. Reactions of a photocatalytic nature depend on various factors that affect the photocatalyst activity and the speed of the degradation process. As a general rule, the activity of the photocatalyst depends fundamentally on the band gap of the material, the recombination rate of the photogenerated e^- / h^+ pairs and the nature of the surface chemical reactions that take place during the illumination of the material. Accordingly, Titanium dioxide is the most widely used semiconductor in the application of processes based on heterogeneous photocatalysis.^{[19][21][22]} Of the three crystalline phases of titanium dioxide existing in nature: anatase, rutile and brookite, only the first two have photocatalytic activity, although the anatase phase generally leads to higher yields in photocatalytic activity.^[22] However, the use of TiO_2 as a photocatalyst also has a series of disadvantages such as its low photoactivity under solar radiation, a high rate of recombination of the e^- / h^+ pairs, and its difficult recovery from the reaction medium due to its small size of particle.^[22]

One option to improve the efficiency of the photocatalytic process is to increase the surface area of the photocatalyst, in order to increase the irradiated surface and improve the contact between the catalyst and the contaminant. With the use of porous materials such as MOFs, it is intended to take advantage of their chemical stability and properties as an adsorbent to improve the catalytic activity of the photoactive species and therefore the efficiency of the process.^[19]

The combination of MOFs and TiO_2 to make TiO_2 -MOF composites show good results in photocatalysis, being better than for the compounds separately^{[20][23]} due mainly to (i) MOFs can play the role of photosensitizer to achieve efficient light utilization; (ii) the photo-excited electrons can be readily transferred from organic linkers to the metal ions or metal cluster; (iii) the semiconductor TiO_2 photocatalyst acts as the primary photocatalysts and some MOFs play the role of co-catalyst.^[23]

2. Methodology

2.1 Reagents, solutions, and materials

For the synthesis of MOFs and composite different salts and organic ligands required: zirconium (IV) chloride anhydrous ($ZrCl_4$, 99%), terephthalic acid (H_2BDC , 98%), 2-aminoterephthalic acid (NH_2-H_2BDC , 99%), mesaconic acid (99%), aluminium nitrate nonahydrate ($Al(NO_3)_3 \cdot 9H_2O$, extra pure), titanium (IV) butoxide (TBT), titanium (IV) oxide (P25), titanium (IV) oxide mixture of rutile and anatase, titanium (IV) oxide, anatase, and (3-aminopropyl) triethoxysilane (APTES), purchased by Sigma-Aldrich. Ultrapure water was obtained through the Milli-Q quality deionized water ($18.2 M\Omega cm^{-1}$) was used, obtained by means of a MilliPore A10 gradient water purification system (Watford, UK), ethanol (EtOH), methanol (MeOH), Urea ($CO(NH_2)_2$, 99%) and succinic acid ($C_4H_6O_4$, 99%) were purchased by Scharlau, whereas hydrochloric acid (HCl, 37%) was acquired from Normapur. N, N-dimethylformamide (DMF) were acquired from Panreac.

For the preparation of the chromatographic mobile phases, Milli-Q quality deionized water ($18.2 M\Omega/cm$) was used, and acetonitrile (ACN) LC-MS grade ChromasolvTM provided by VWR International (Barcelona, Spain).

The evaluation of the extractive capacity of the materials obtained was raised by determining six personal care products (PCPs): methylparaben (MPB), ethylparaben (EPB) and propylparaben (PPB) acquired from Dr Ehrenstorfer GmbH (Augsburg, Germany), and benzylparaben (BzPB), benzophenone (BP) and 3 benzophenone (3-BP) purchased from Sigma Aldrich.

2.2 Characterization

The powder x-ray diffraction (PRDX) patterns of the composite material was collected on an Empyrean diffractometer to determine their crystallographic structure. A spectrometer Avatar 360 Ft-IR was employed for the infrared spectra. Thermogravimetric analysis (TGA) curves were recorded with a Pyris Diamond TG/TGA of Perkin Elmer and conditions: at a heating rate of $10\text{ }^\circ\text{C}/\text{min}$ under a N_2 flow rate of $50\text{ mL}/\text{min}$; the temperature ranged from room temperature to $600\text{ }^\circ\text{C}$. Micromeritics ASAP 2020 analyzer was used for the Brunauer-Emmett-Teller (BET) surface area of the samples. Scanning electron microscopy (SEM, Zeiss Evo 15), energy-dispersive X-ray (EDX) were used to determine the morphology, size, and elemental distribution of the materials. Dynamic light scattering (DLS) to analyze particle size were collected on Zetasizer Nano ZD de Malvern instruments. Chromatographic analysis was performed with a 1260 Infinity high performance liquid chromatograph (HPLC) from Agilent Technologies (Santa Clara, CA, USA) equipped with a quaternary pump, a Rheodyne 7725i injection valve with a $20\text{ }\mu\text{L}$ loop, an EC-C18 InfinityLab PoroShell column ($50\text{ mm} \times 4.6\text{ mm} \times 2.7\text{ }\mu\text{m}$) supplied by Agilent Technologies and a ProStar 325 LC UV-Vis detector from Varian (Palo Alto, CA, USA).

2.3 Synthesis of MOFs

2.3.1. UiO-66 (Zr)

This compound has been synthesized according to the procedure reported by Katz et al.^[24] UiO-66 was performed by dissolving zirconium (IV) chloride anhydrous (ZrCl₄, 1 mmol) and benzene-1,4-dicarboxylic acid (H₂BDC, 2 mmol) in N, N-dimethylformamide (DMF, 15 mL) and concentrated hydrochloric acid (HCl, 1 mL). The resulting mixture was heat at 150 °C for 24 h. After that, the solution was cooled down to room temperature and filtered. The MOF was activated repeatedly washed with DMF and methanol and heated at 80 °C for 24 h.

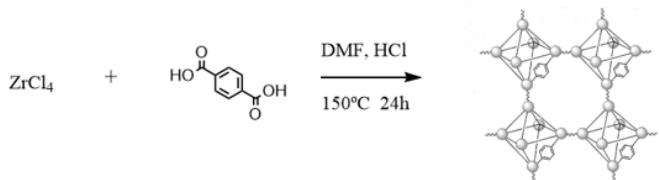


Fig 1a. UiO-66 MOF structure. Metal and ligand precursors^[24]

2.3.2. UiO-66-NH₂(Zr)

This MOF was synthesized analogously by replacing H₂BDC with the equivalent molar amounts of 2-aminoterephthalic acid (NH₂-H₂BDC, 2 mmol).

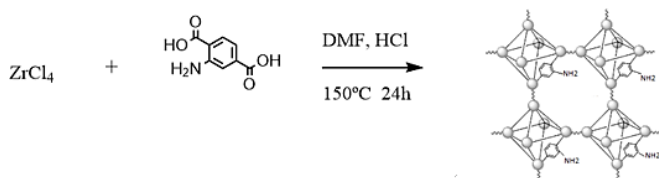


Fig 1b. UiO-66-NH₂ MOF structure. Metal and ligand precursors^[24]

2.3.3. CIM-80 (Al)

This compound has been synthesized according to the following procedure.^[16] The synthesis requires a mixture of mesaconic acid (1 mmol) and aluminium nitrate nonahydrate (Al(NO₃)₃·9H₂O, 1 mmol) in deionized water (15 mL) containing urea (0.5 mmol), under constant stirring. Then, the resulting mixtures was heat at 150 °C for 24 h. After the solution was cooled down to room temperature and filtered. The MOF was activated repeatedly washed with deionized water and heated at 80 °C for 24 h.

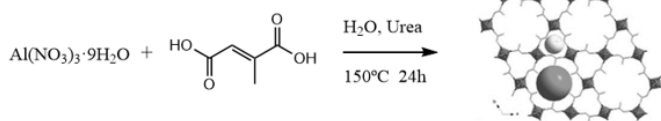


Fig 1c. CIM-80 MOF structure. Metal and ligand precursors.^[22]

2.4 Synthesis of Composite

Different strategies have been followed for the synthesis of the different composites:

- Strategy 1:** MOF @ TiO₂ core-shell structure, where the MOF is surrounded by the photocatalyst.
- Strategy 2:** TiO₂ @ MOF core-shell structure, *in situ* approach, where the photocatalyst is surrounded by the MOF using a one-step hydrothermal method.

(c) **Strategy 3:** TiO₂ @ MOF core-shell structure, functionalization process. This was done using a mild synthetic procedure by functionalizing the photocatalyst.

Summary of the obtained composites and synthetic procedures followed in each case:

Table 2. Name, MOF and TiO₂ precursors used for the formation of the different composites and their synthetic procedures.

Composite Name	MOF	TiO ₂
UiO-66 @ TiO ₂ (30%) (1)	UiO-66 (Zr)	TBT*
UiO-66-NH ₂ @ TiO ₂ (30%) (2)	UiO-66-NH ₂ (Zr)	TBT
CIM-80 @ TiO ₂ (30%) (3)	CIM-80 (Al)	TBT
UiO-66 @ TiO ₂ (50%) (4)	UiO-66 (Zr)	TBT
UiO-66-NH ₂ @ TiO ₂ (50%) (5)	UiO-66-NH ₂ (Zr)	TBT
CIM-80 @ TiO ₂ (50%) (6)	CIM-80 (Al)	TBT
Ultrasound treatment and hydrothermal method were adopted to prepare 1-6 with UiO-66, UiO66-NH ₂ , CIM-80 and tetrabutyl titanate as precursors		
P21 @ UiO-66 (7)	UiO-66 (Zr)	P21**
One-step hydrothermal method was adopted to prepare P21 @ UiO66 with ZrCl ₄ , titanium (IV) oxide anatase, and amino-terephthalic acid as precursors.		
P25 @ UiO-66 (8)	UiO-66 (Zr)	P25**
One-step hydrothermal method was adopted to prepare P25 @ UiO66 with ZrCl ₄ , titanium (IV) oxide (P25), and amino-terephthalic acid as precursors.		
P100 @ UiO-66 (9)	UiO-66 (Zr)	P100**
One-step hydrothermal method was adopted to prepare P100 @ UiO66 with ZrCl ₄ , titanium (IV) oxide mixture of rutile and anatase, and amino-terephthalic acid as precursors.		
P21 @ UiO-66-NH ₂ (10)	UiO-66-NH ₂ (Zr)	P21
One-step hydrothermal method was adopted to prepare P21 @ UiO66-NH ₂ with ZrCl ₄ , titanium (IV) oxide anatase, and 2- amino-terephthalic acid as precursors.		
P25 @ UiO-66-NH ₂ (11)	UiO-66-NH ₂ (Zr)	P25
One-step hydrothermal method was adopted to prepare P25 @ UiO66-NH ₂ with ZrCl ₄ , titanium (IV) oxide (P25), and 2- amino-terephthalic acid as precursors.		
P100 @ UiO-66-NH ₂ (12)	UiO-66-NH ₂ (Zr)	P100
One-step hydrothermal method was adopted to prepare P100 @ UiO66-NH ₂ with ZrCl ₄ , titanium (IV) oxide mixture of rutile and anatase, and 2- amino-terephthalic acid as precursors.		
TiO ₂ -COO @ UiO-66 (13)	UiO-66	P25
TiO ₂ -COO @ UiO-66-NH ₂ (14)	UiO-66-NH ₂	P25
The mixture prepared with the TiO ₂ particles functionalized with carboxylic groups and MOF building block was heated at 80 °C for 24 h.		
TiO ₂ -COO @ CIM-80 (15)	CIM-80 (Al)	P25
The mixture prepared with the TiO ₂ particles functionalized with carboxylic groups, Al(NO ₃) ₃ ·9H ₂ O, mesaconic acid, urea and H ₂ O was heated at 150 °C for 24 h.		

*TBT = tetrabutyl titanate.

**P25 = titanium oxide particles (mixed phases, size 21 nm); P21 = titanium oxide particles (pure phase, size <25 nm); P100 = titanium oxide particles (mixed phases, size 100 nm)

2.4.1. MOF @ TiO₂ Core - shell structure

UiO-66 @ TiO₂ (30%) (1); UiO-66-NH₂ @ TiO₂ (30%) (2); CIM-80 @ TiO₂ (30%) (3); UiO-66 @ TiO₂ (50%) (4); UiO-66-NH₂ @ TiO₂ (50%) (5) and CIM-80 @ TiO₂ (50%) (6) are isolated following the same synthetic method:

MOF @ TiO₂ composite were produced via a hydrothermal synthesis, following the previously reported method^[25]. To get 30% by weight of MOF, 50 mg of MOF was dispersed in titanium (IV) butoxide (TBT, 2 mL) and ethanol (EtOH, 8 mL). The above mixture was ultrasonically treated for 10 minutes, before ultrapure water (0.4 mL) was added into the suspension. The suspension was then transferred to a Teflon-lined at 180 °C for 20 hours. Finally, it was cooled down at room temperature, washing with ethanol and was dried at 80 °C for 24 hours.

For 50% by weight of MOF the same procedure was followed but using 0.5 mL of TBT.

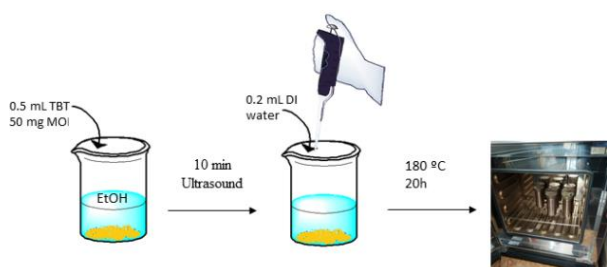


Fig 2a. Scheme of the synthetic procedure followed for the synthesis of **UiO-66 @ TiO₂ (30%) (1)**; **UiO-66-NH₂ @ TiO₂ (30%) (2)**; **CIM-80 @ TiO₂ (30%) (3)**; **UiO-66 @ TiO₂ (50%) (4)**; **UiO-66-NH₂ @ TiO₂ (50%) (5)** and **CIM-80 @ TiO₂ (50%) (6)** composites

2.4.2. TiO₂ @ MOF Core-shell structure by a *in situ* approach

P21 @ UiO-66 (**7**); P25 @ UiO-66 (**8**); P100 @ UiO-66 (**9**); P21 @ UiO-66-NH₂ (**10**); P25 @ UiO-66-NH₂ (**11**); P100 @ UiO-66-NH₂ (**12**) are isolated following the same synthetic method:

According to the literature procedure [26] we obtain the composite for UiO-66 and UiO-66-NH₂. For the titanium oxide particles used, the size and phase have been modified, naming them as follows: P21 (Anatase phase, size <25 nm), P25 (Anatase and Rutile phases, size: 21 nm) and P100 (Anatase and Rutile phase, size: 100 nm).

0.25 g of those preformed TiO₂ particles were dispersed in *N,N*-dimethylformamide (DMF, 15 mL) solution and kept stirring. Meanwhile, zirconium (IV) chloride anhydrous (ZrCl₄, 1 mmol), benzene-1,4-dicarboxylic acid (H₂BDC, 2 mmol), hydrochloric acid (HCl, 1 mL) were successively added to the solution and stirred for 30 min at room temperature. The obtained solution was loaded into a Teflon-lined autoclave and heated at 140 °C for 24 h. The final product was collected, washing, and ensuring drying in a stove at 80 °C for 24 h. In the case of UiO-66-NH₂, the same procedure has been used by replacing H₂BDC with the equivalent molar amounts of 2-aminoterephthalic acid (NH₂-H₂BDC, 2 mmol).

On the other hand, 0.25 g preformed TiO₂ particles was first mixed with aluminium nitrate nonahydrate (Al(NO₃)₃·9H₂O, 2.3 mmol/L) aqueous solution for the synthesis of the CIM-80 composite compound [27]. Then, it was heated and stirred by a hotplate stirrer at 95 °C and 1200 rpm for 2 h. After that, the powders were washed by deionized (DI) water through the centrifugation/redispersion process to remove the iron residues. Subsequently, the powders were redispersed in DI water (5 mL) together with mesaconic acid (2.3 mmol/L) and Urea (1.15 mmol/L). After vortex mixing, the mixtures were poured into a Teflon-lined autoclave, which was then put in a stove at 150 °C for 24 h. Finally, the composite products were obtained after washing with deionized water through several centrifugation/redispersion processes.

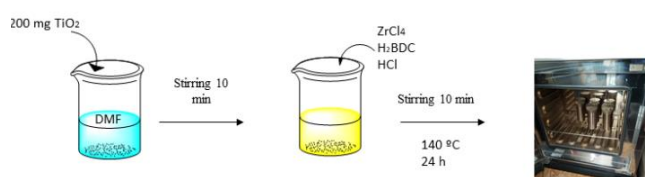


Fig 2b. Scheme of the synthetic procedure followed for **P21 @ UiO-66 (7)**; **P25 @ UiO-66 (8)**; **P100 @ UiO-66 (9)**; **P21 @ UiO-66-NH₂ (10)**; **P25 @ UiO-66-NH₂ (11)**; **P100 @ UiO-66-NH₂ (12)** composites

2.4.3. TiO₂ @ MOF Core-shell structure by a TiO₂ functionalization process

TiO₂-COO @ UiO-66 (**13**); TiO₂-COO @ UiO-66-NH₂ (**14**); TiO₂-COO @ CIM-80 (**15**) are isolated following the same synthetic method:

Titanium oxide preformed particles were previously functionalized with carboxylic group following different literature procedures [28,29], to then synthesize the different MOF on the surface.

0.45 g of succinic acid and APTES (1 mL) were dissolved in *N,N*-dimethylformamide (DMF, 30 mL) by stirring for 3 hours. Then, deionized (DI) water (2 mL), DMF (10 mL) and 0.5 g preformed TiO₂ were added, keeping it stirring for 8 hours. The final product was washing with ethanol.

For the growth of the different MOFs, the functionalized particles were dispersed in 10 mL of DMF with the aid of the stirrer. Then, 2 mM of the metal salt was dissolved in 5 mL of the solvent and added dropwise to the previous solution. Finally, the same procedure was carried out with the organic molecule ligand. The obtained solution was loaded into Teflon-lined autoclave and heated at 80 °C for 24 h. Finally, the composite products were obtained after several washing processes and separated by centrifugation. The CIM-80 composite sample was obtained with the same synthetic procedure but using H₂O as a solvent and the solution was heated at 150 °C for 24 h.

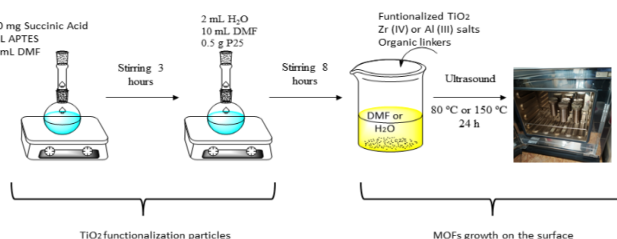


Fig 2c. Scheme of the synthetic procedure followed for **TiO₂-COO @ UiO-66 (13)**; **TiO₂-COO @ UiO-66-NH₂ (14)**; **TiO₂-COO @ CIM-80 (15)** composites

2.5 Adsorption analytes

To evaluate the extractive capacity of MOF and derived composites, a comparative study was carried out between the results obtained in the determination of a set of personal care products (PCPs) using the synthesized materials and their individual components.

According to the literature procedure [30] the chromatographic separation was carried out at room temperature using a binary mobile phase made up of ACN and Milli-Q water with 0.1% acetic acid, at a constant flow of 0.5 mL/min. For optimal separation and determination, the following elution gradient was applied: it was started with 50% ACN, which was kept constant for 1 minute. Then the percentage of ACN was gradually increased from 50 to 90 % in 8 minutes and finally to 100 % in 1 minute. Subsequently, the percentage of ACN was progressively reduced to 50 % in 5 minutes and was kept at this value for a further 1 minute, achieving a total injection time of 16 minutes. Detection and quantification of the analytes was achieved by setting the measurement wavelength at 254 nm.

3. Results / Discussion

Two zirconium MOFs (UiO-66 and UiO-66-NH₂), an aluminium MOF (CIM-80), and different types of titanium oxide particles were used for the formation of new composites through different synthetic strategies. The amino (-NH₂) functional group was chosen to be representative of polar functionality. Following an isorecticular synthesis, a family of UiO-66-X composites was obtained from the two different linker ligands: H₂BDC and NH₂-H₂BDC. CIM-80 was used due to its stability, its facile and benign synthesis, and its structural rigidity. For the titanium oxide particles used, the size and phase have been modified, naming them as follows: P21 (Anatase phase, size: <25 nm), P25 (Mixture of Anatase and Rutile phases, size: 21 nm) and P100 (Mixture Anatase and Rutile phases, size: 100 nm), to analyze the influence of these parameters in the physical-chemical properties of the final compounds. In total, 15 new composites were prepared by the combination of the 3 MOFs and the different types of TiO₂ particles. (Fig 3) The reaction conditions have been modified with respect to the previous published synthesis in order to optimize the preparation. All composites were obtained in high yields without loss of crystallinity of their components.



Fig 3. Scheme of the synthetic procedure followed for the fabrication of composites 1-15

The control of the composition and shape is of great importance to obtain a particular composite under reproducible conditions, but it is also well known that this is not always easy to achieve. In this sense, we have attempted to control the preparation of the different composites through the investigation of several synthetic variables. The different types of composites based on the MOFs/TiO₂ systems (MOFs = UiO-66-X or CIM80) were obtained by adjusting the synthetic conditions. These compounds are listed in Table 2 and Fig 3. Generally, the presynthesized core material was first prepared prior to growth of the compound shell around, resulting in discrete core-shell species.

To achieve core-shell structures where the MOF was surrounded by the photocatalyst the first synthetic strategy was followed (Fig 4a). Here, the synthesis and characterization of MOFs compounds were previously done, following with the coated with TiO₂ *in situ* synthesized from titanium butoxide precursor. The MOF/TiO₂ ratio of the composites was controlled by altering the mass of titanate present in the synthesis.

A second strategy was followed to isolate composites where the preformed photocatalyst were surrounded by the different MOFs (Fig 4b). For this purpose, the direct growth of the MOF on the surface of the titanium oxide particles was carried out in a one-step synthesis, where the MOF and the composite were simultaneously obtained.

Functionalization of the titanium oxide particles with carboxylic groups was also done, followed by an *in situ* growth method to

synthesize the MOFs on their surface. This strategy was followed to guarantee that the MOF remains bound to the TiO₂ particles. Furthermore, a mild synthetic procedure was used to control the size of the particles (see 2.4.3 section). The formation of the UiO-66-X composites was based on the previously reported method but applying much lower temperature (80 °C) to suppress MOF formation in the bulk solution. It was not possible to isolate CIM-80 at this temperature.

The activation of the composites was carried out by washing several times with ethanol and drying in an oven at 80 °C for 24 h. In the case of compound 15, water was used.

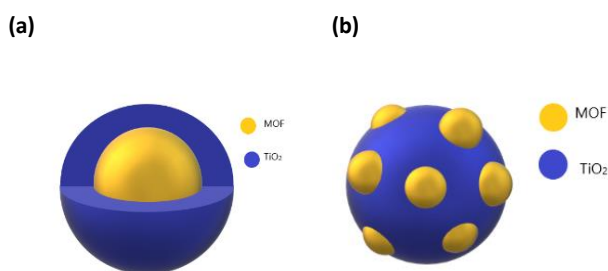


Fig 4. Representation of the different core-shell structures: (a) MOF @ TiO₂ and (b) TiO₂ @ MOF

3.1 Characterization of MOFs

The synthesized MOFs have been characterized by X-ray powder diffraction (PDRX), FT-IR spectrum and Nitrogen adsorption isotherms.

MOFs compounds were obtained through different solvothermal or hydrothermal methods and, whereas the synthesis could be scaled up without loss of crystallinity or porosity in UiO-66 and UiO-66-NH₂, it was not possible to scale up the synthesis of CIM80.

UiO-66 is a zirconium-based MOF built up from hexamers of eight coordinated ZrO₆(OH)₂ polyhedra and terephthalate ligands. The correct structure of MOFs UiO-66 and UiO-66-NH₂ was verified by comparing the activated synthesized material and the theoretical PDRX patterns [21]. Comparing the obtained pattern and the theoretical one, confirming the correct formation of UiO-66 and UiO-66-NH₂. (See Fig. S5a) X-ray diffraction revealed that the two compounds are isostructural with the parent material UiO-66 topologically equivalent with UiO-66-NH₂. It is important to proof this equivalence in order to achieve proper comparison. The crystallinity structure of the samples after the activation procedures was also confirmed by X-ray powder diffraction.

The presence of the functional groups on the linkers was further evidenced by characterizing the MOFs with FTIR spectroscopy (See, Fig. S6a and b). Thus, UiO-66-NH₂ displays a broad absorption band at 2930 cm⁻¹ that is assigned to the N-H stretching modes. In general, the infrared spectrum data show the characteristic peaks of the aromatic rings and carboxyl groups in the 1350-1600 cm⁻¹ region. The strong IR bands between 1600 and 1640 cm⁻¹ can be assigned to the ν_{asym}(OCO) vibration mode and the medium intensity bands at around 1360 cm⁻¹ are attributable to the ν_{sym}(OCO) vibration mode. N₂ adsorption/desorption isotherms were collected at 77 K and the Brunauer, Emmett and Teller (BET) surface areas were calculated, and all the materials were found to retain porosity. The BET surface area data was found to decrease in surface area with the functionalization of the pores, from ~1342 m²·g⁻¹ in the parent UiO-66 to ~794 m²·g⁻¹ for UiO-66-NH₂.

The CIM-80 was characterized by PDRX pattern, establishing a comparative study with the theoretical diffractogram of the bibliographic reference.^[12] The obtained pattern and the theoretical one confirming the correct formation of CIM-80. (See Fig. S5b)

The presence of the carboxylic groups on the mesaconic linkers was also evidenced by characterizing the MOFs with IR spectroscopy (Fig. S6c)

The crystal lattice of CIM-80 (Al) is made up of octahedral structures of AlO_6 that interconnect through -OH groups and mesaconate molecules, giving rise to the formation of two different types of pores: one hexagonal and the other trigonal, of 6 and 2 Å in diameter respectively. N_2 adsorption/desorption isotherms were collected at 77 K leads to a BET surface area for this material of $891 \text{ m}^2 \text{ g}^{-1}$.

3.2 Structural characterization of Composites

3.2.1. MOF @ TiO_2 core- shell structure (1-6)

The synthesized composites have been characterized by the following techniques: X-ray powder diffraction, Nitrogen adsorption isotherms, DLS and thermogravimetric analysis.

The composites exhibit good thermal and chemical stability in water. The MOF/ TiO_2 ratio of the composites was controlled by altering the mass of titanate present in the synthesis. The nature of the as-synthesized materials was confirmed by a comparison of the experimental X-ray diffraction patterns with the theoretical results of different MOFs or TiO_2 phases. DRX pattern showed the presence of the corresponding MOFs compound and the anatase phase of the titanium oxide in 1-6 composites (see Fig S7a, c). Among the three natural crystalline forms of TiO_2 , pure phase of anatase was always observed. Noteworthy, anatase phase TiO_2 has superior optoelectronic and photochemical properties.^[25]

The decomposition of the composite can be observed as we increase the temperature by means of TGA analysis. In general, three different regions are distinguished: A first region, between r.t. and 100°C , where the elimination of the free organic molecules and the guest solvents (H_2O , DMF ...) occurs; a second region, a plateau between 100 and 400°C , corresponding to the thermal stability of the MOF; and a last region, between 400 and 600°C , where the organic decomposition take place and the inorganic residual part of the compound is found (titanium dioxide and metal oxides). The MOFs/ TiO_2 weight ratio in 1-6 was estimated by TGA analysis, showing a slightly lower value than expected for the cases of UiO-66 and UiO-66-NH₂, around 20 % and 15% for the compounds 1 and 2 and 35% and 30% for the compounds 4 and 5 respectively. On the other hand, the weight percent of the originally synthesized ratio is found in CIM-80 derivatives 3 and 6. (see Fig 5a, b)

Table 3 shows the surface area of these MOFs, which was calculated using the N_2 adsorption isotherms, providing us with information on the porosity of our compound. BET surface areas between 633 - $275 \text{ m}^2 \text{ g}^{-1}$ showed that 1, 2, 5, 6 composites possessed some degree of porosity, which, as we expected, were lower than pure MOFs because of the occupation of TiO_2 crystals in or out of the different MOFs pores. On the other hand, the surface area of composite 3 was markedly decreased, forming a non-porous compound. This dramatically decreased compared to the pure CIM-80, indicating that TiO_2 nanocrystals were not only coated out of the MOF surface, but also incorporated into the inner pores of CIM-80.

Dynamic light scattered (DLS) measurements showed that the average particle size was between 4062 nm in 2 and 143 nm in 6.

Table 3. BET surface area, particle size and % MOF/ TiO_2 for UiO-66 @ TiO_2 (30%) (1); UiO-66-NH₂ @ TiO_2 (30%) (2); CIM-80 @ TiO_2 (30%) (3); UiO-66 @ TiO_2 (50%) (4); UiO-66-NH₂ @ TiO_2 (50%) (5) and CIM-80 @ TiO_2 (50%) (6)

MOF – TiO_2	BET Surface area (m^2/g)	Particle size (nm)	% MOF/ TiO_2
UiO-66 @ TiO_2 (30%) (1)	276	1000	20
UiO-66-NH ₂ @ TiO_2 (30%) (2)	275	4062	15
CIM-80 @ TiO_2 (30%) (3)	2	1000	30
UiO-66 @ TiO_2 (50%) (4)	429	948	35
UiO-66-NH ₂ @ TiO_2 (50%) (5)	-*	309	30
CIM-80 @ TiO_2 (50%) (6)	643	143	45

*Compound 5 has not been characterized by N_2 adsorption

Composites with higher amounts of MOFs (4,5,6) increase the surface areas and also showed smaller particles size, probably the amount of MOF used, effectively prevents particle aggregation during the material preparation (Table 3).

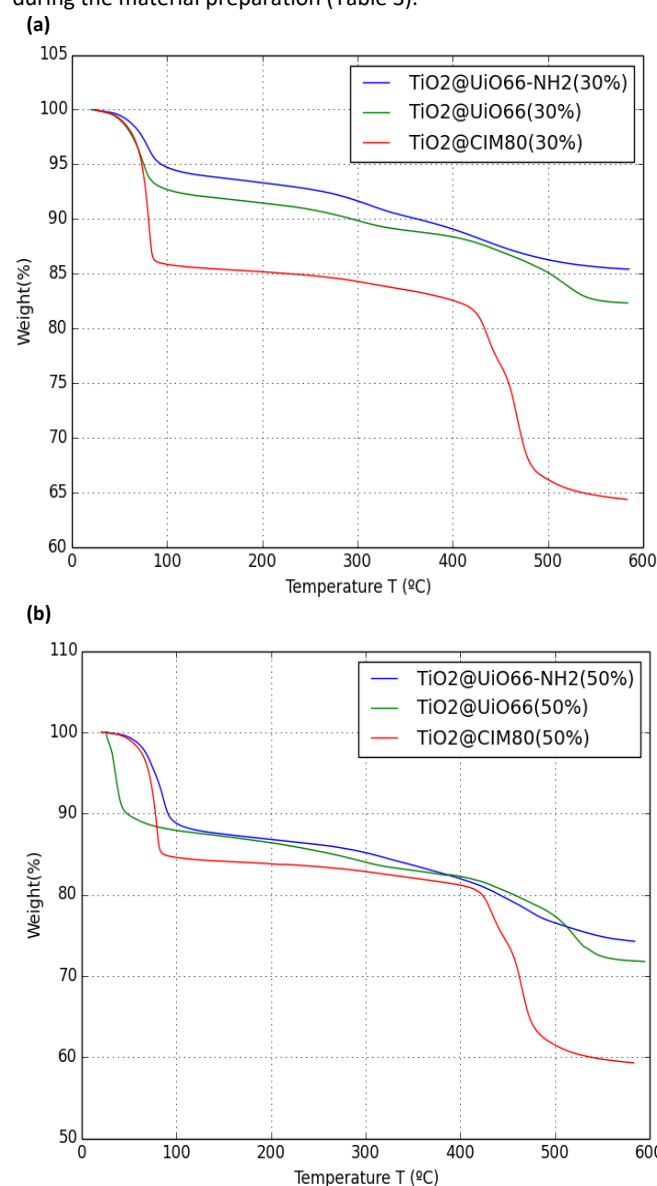


Fig 5. TGA of (a) TiO_2 @ UiO-66(30%) (1), TiO_2 @ UiO66-NH₂(30%) (2) TiO_2 @ CIM-80(30%) (3) composites and (b) TiO_2 @ UiO66-NH₂(50%) (4), TiO_2 @ UiO66 (50%) (5), TiO_2 @ CIM-80 (50%) (6) composites

3.2.2. TiO₂ @ MOF core shell structure *in situ* approach (7-12)

The synthesized composites have been characterized by the following techniques: X-ray powder diffraction, Nitrogen adsorption isotherms, DLS, and thermogravimetric analysis.

For the *in situ* approach, six different composites have been obtained depending on the titanium oxide particles used. The size and phase have been modified, naming them as follows: P21 (Anatase phase, size <25 nm), P25 (Anatase and Rutile mixture phases, size 21 nm) and P100 (Anatase and Rutile mixture phase, size 100 nm). In the case of CIM-80 composite no signals of MOF formation could be detected. The composites exhibit good thermal and chemical stability in water.

The presence of MOFs and the different phases of titanium oxide in the crystalline structure was also confirmed performing study by X-ray powder diffraction pattern, so we can confirm with the Fig 6a-b their correct synthesis. For the particles P25 and P100, the anatase and rutile phases were presented, while for the P21 the pure anatase phase was detected. Through a TGA analysis, the real relationship between the weight of the MOF and the TiO₂ could be calculated, being around 60% for all cases. (See Fig S10a-b) These results reveal that the TiO₂ phase or size precursor do not clear influence the composition of the formed composites.

Table 4 shows the average particle size, which was calculate using the dynamic light scattered (DLS) measurements. The average particle size was between 1031 nm in **12** and 2171 nm in **11**.

Table 4. Particle size for P21 @ UiO-66 (**7**); P25 @ UiO-66 (**8**); P100 @ UiO-66 (**9**); P21 @ UiO-66-NH₂ (**10**); P25 @ UiO-66-NH₂ (**11**); P100 @ UiO-66-NH₂ (**12**)

MOF @ TiO ₂	Particle size (nm)
P21 @ UiO-66 (7)	1824
P25 @ UiO-66 (8)	1431
P100 @ UiO-66 (9)	1144
P21 @ UiO-66-NH ₂ (10)	1611
P25 @ UiO-66-NH ₂ (11)	2171
P100 @ UiO-66-NH ₂ (12)	1031

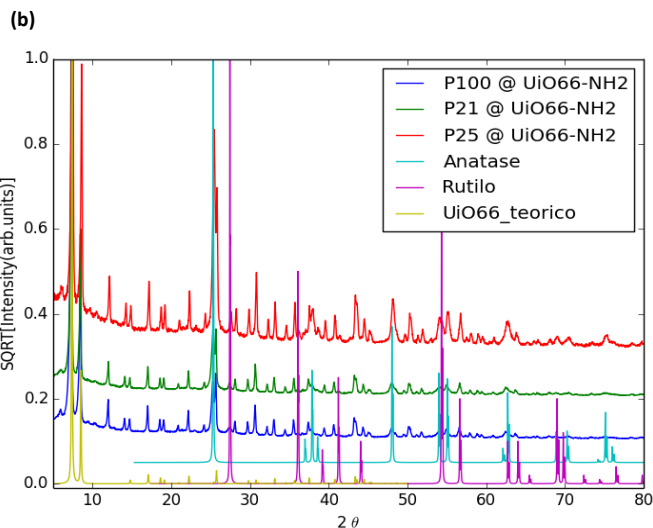
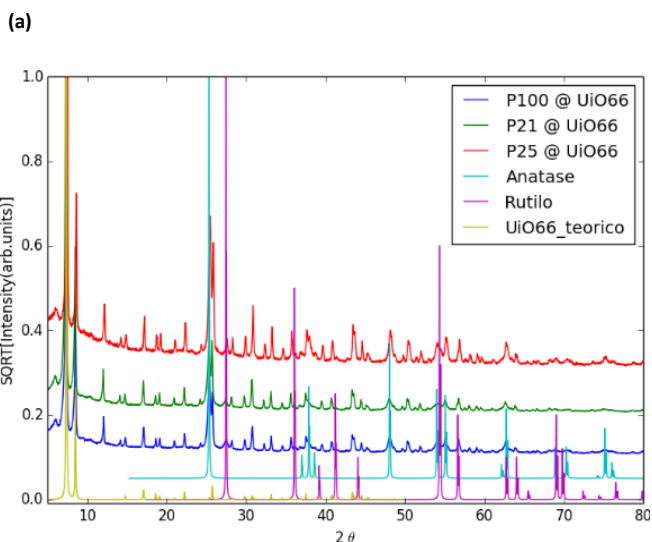


Fig 6. X-ray powder diffractogram of (a) P21 @ UiO-66 (**7**); P25 @ UiO-66 (**8**); P100 @ UiO-66 (**9**) composites and for (b) P21 @ UiO-66-NH₂ (**10**); P25 @ UiO-66-NH₂ (**11**); P100 @ UiO-66-NH₂ (**12**) composites

3.2.3. TiO₂ @ MOF core shell structure functionalization process (13-15)

The synthesized composites have been characterized by the following techniques: X-ray powder diffraction, and FT-IR spectrum.

In this procedure, a first functionalization of the titanium oxide particles was carried out in order to guarantee that the growth of the MOF occurs around the photocatalyst. In addition, the mildest synthetic procedure was used to control the particle size. In the case of **15**, the characterization of the composite could not be performed. Through FT-IR spectrum the presence of the carboxylic groups could be detected. The carboxylic band at a wavelength of 1556 cm⁻¹ and in the strong band in the region of 460-700 cm⁻¹, attributed to titanium oxide, confirming the functionalization of the photocatalyst with the carboxyl group. (See Fig S11) The growth of the MOF could be confirmed by X-ray powder diffraction (See Fig S12) and the IR spectrum (see Fig S13).

3.3 Morphology of Composites

SEM analysis is a tool that uses a focused electron beam to produce complex, high-magnification images of sample's surface topography. With this technique we hope to obtain the morphology of the new composites, which are expected to be spheres due to the presence of titanium. Elemental mapping and energy dispersive spectroscopy (EDX) have been used for compositional analysis of the desired samples. [31] According to the strategy used in this work, we expect to obtain the aluminum surrounding the titanium for the compounds **1-6** obtained from the first strategy, while for the rest of the compound the titanium should be surrounding the aluminum.

SEM characterization could not be obtained for most composites except for the case of CIM-80 @ TiO₂ (30%) (**3**), the Fig 7 show a scanning electron microscope (SEM) study in which we can verify the expected morphology of the composites. It consists of spheres of a heterogeneous mixture of components, where the titanium spheres are in varying sizes. The EDS mapping of **3** indicates that the green and red dots assigned to the Ti and O elements (Fig 7c, 7d), respectively, were homogeneously distributed under the pink dots of Al elements (Fig 7b) forming core-shell particles.

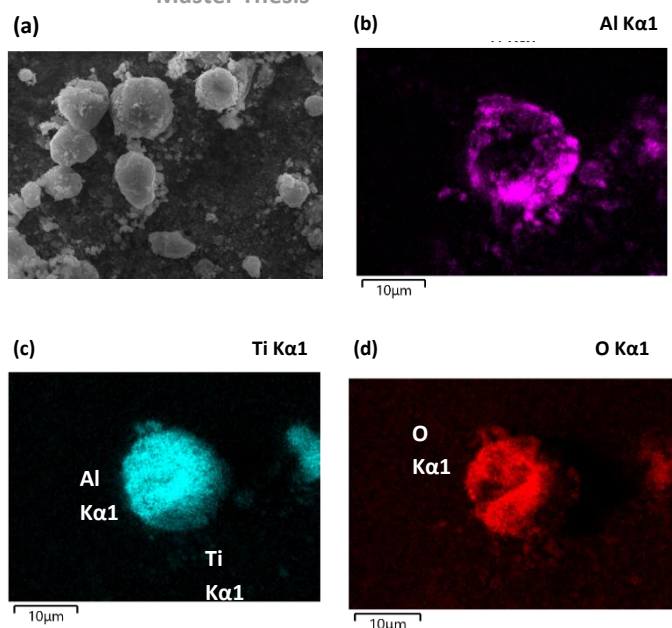


Fig 7. (a) SEM of CIM-80@TiO₂ (30%) (**3**) and elemental mapping of composite (b) aluminium, (c) titanium, (d) oxygen.

3.4 Adsorption properties for PCP

The main analytical parameters of the chromatographic method are shown in (Table S5). The coefficients of determination (R^2) obtained are equal to or greater than 0.9993, reflecting the adequate linearity of the method. The limits of detection (LOD) and quantification (LOQ) are estimated by means of the relationship signal/noise (S/N) as 3-S/N and 10-S/N respectively, being verified experimentally by injecting standards at the estimated concentrations. The LODs and LOQs are between 0.75 - 3 $\mu\text{g/L}$ and 2.5 - 10 $\mu\text{g/L}$. The precision of the chromatographic method is studied by verifying its repeatability ($n=3$) and intermediate precision ($n=9$) at two concentration levels during 3 consecutive days of testing, achieving maximum standard deviations (RSDs) of 10.1% and 6.97% at a low level of 40 $\mu\text{g/L}$ and 1.59% and 1.99% at a high concentration level of 350 $\mu\text{g/L}$.

After completion of the optimization, the chromatographic method was carried out using the different composites as sorbents. In Fig 8 the comparison is shown in terms of extraction efficiency, reflected as the μg of analyte extracted/ mg MOF obtained for each analyte. Compounds **7,9,10** and **12** have not been considered since the change in titanium oxide particles does not affect the coating as we had seen previously.

The obtained results, show in Fig 8, revealed that UiO66-NH₂ and its composites were the best compounds as sorbent for 4 out of the 6 contaminants studied, and thus it can be considered a generic sorbent if intending a multi-component determination. As expected, pristine TiO₂ (P25) compound showed poor extraction values, indicating the importance of the porosity for microextraction procedures. In general, the UiO-66-X composites presented the best extractive capacities for the six selected PCPs, although with lower values than bare MOFs. However, although the combination between MOFs and TiO₂ led to the decrease of the total surface areas, the different isolated composites still exhibited good extractive capacities. On the other hand, for the case of CIM-80 and derived composites, lower extractive capacities were presented, which improve when forming the composites. Composites **3-6**, with higher amounts of MOFs in their composition than **1-3**, and consequently, higher surface areas, do not show better extraction values. This could be due to the MOF @ TiO₂ core-shell structure,

where the TiO₂ shell could block the pore space required for the optimal diffusion of the contaminant molecules. The results indicate that composite **11** showed better extraction values towards MPB, EBP and PPB organic pollutants in spite of the lower porosity compared to pure UiO66-NH₂, and in general, this composite showed the best extraction performances for the tested group of analytes.

Mostly, the functionalization by polar groups is a factor positively affects the total efficiency of the method for the studied analytes of quite different nature. This result shows that the reduction in effective pore size by functional groups is not critical in the analytical procedure, since the electronic properties of these groups favour the analyte-MOF interaction.

The positively influenced on the extraction efficiency due to the presence of functionalization groups in the ligands of UiO-66 has already been studied.^[11] Here, the same behavior is observed in the different UiO66-NH₂ composite compounds.

Overall, TiO₂ @ MOF composites are the best extractant materials and the best extraction performance occurs for **11** with benzylparaben (BzPB) and 3-Benzophenone (3-BP) molecules. The extraction values for this composite follow the trend BzPB > MPB \approx PBP > EBP and 3-BP > BP, probably following the trend of the higher hydrophobic character and lower solubility in water of the different organic pollutants. This result indicates that hydrophobic interactions can make a critical difference during the extraction process. The possible explanation for the good results observed in TiO₂ @ MOF composites (**8** and **11**) could be attributed to the core-shell architectures, where the MOFs are located in the shell of the structures with accessible pore space for the different organic pollutants.

The results observed in **13** and **14** indicate that the synthetic procedure followed in TiO₂ @ MOF structures by a TiO₂ functionalization is a noteworthy factor negatively affecting the total efficiency of the method for the studied analytes.

In some composites, made with UiO-66 and its functionalized version, the EPB was masked, possibly due to the residual ligand.

It is difficult to establish relationships between the effects of the composition formation of MOFs on their sorption capacities because there are numerous factors to consider that make each system different^[32]. The precise control of the guest location is in most cases not possible and depositing guests on the MOFs external surfaces is unavoidable^[33]. However, the observed results show that a suitable porosity is necessary to use composite-MOFs compounds as generic sorbents in analytical processes.

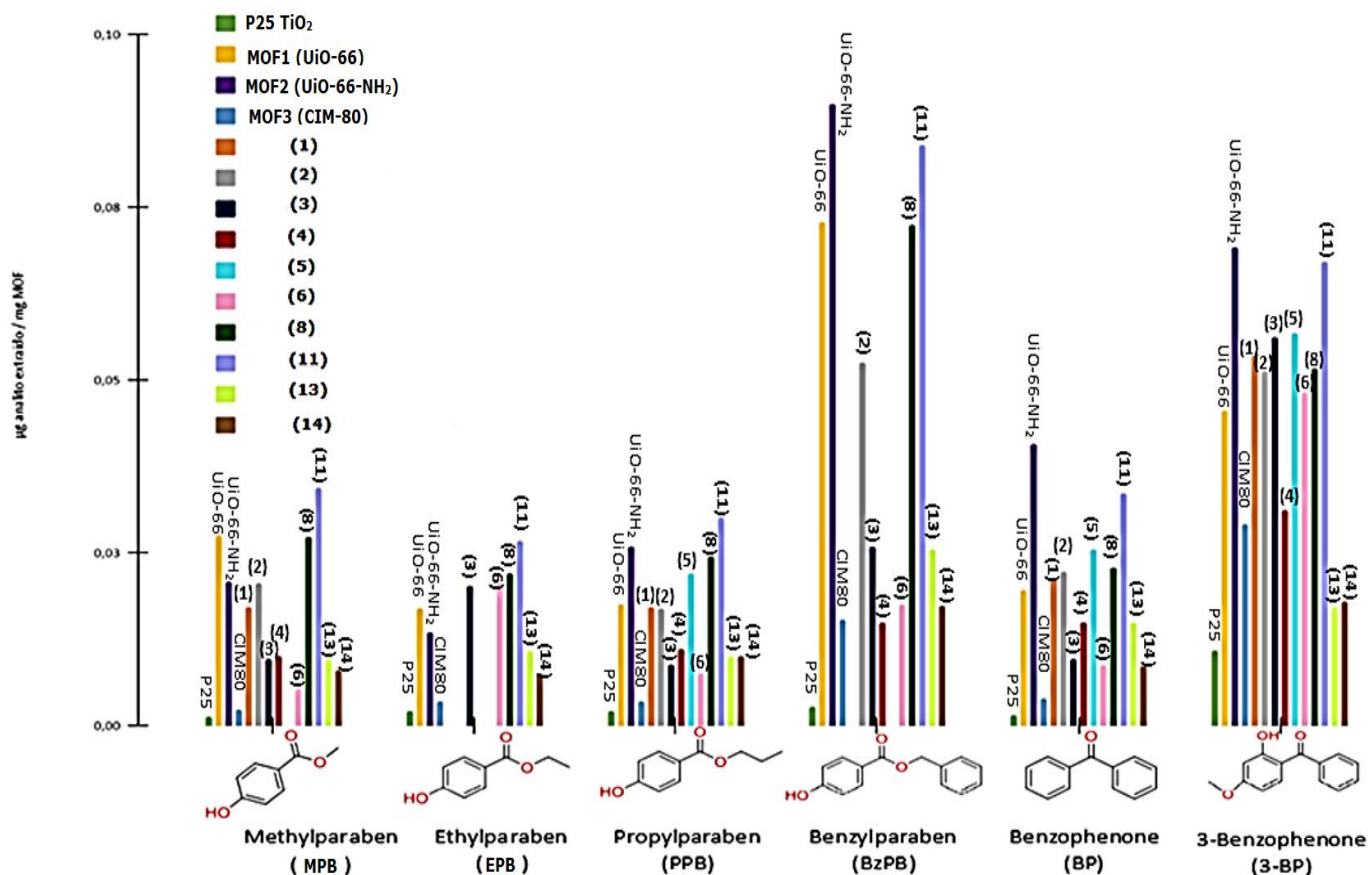


Fig 8. Comparison between the different composites and precursors used in terms of extraction efficiency for each analyte

4. Future Work

The last objective of this work would be the study of the photocatalytic activity for the degradation of analytes adsorbed by composites, with the purpose of eliminate the emerging pollutants and obtain a reusable material.

For this, the new synthesized composites will be used, where titanium oxide was used as a photocatalyst and MOFs to improve efficiency by increasing the surface area in order to increase the irradiated surface and improve the contact between the catalyst and the contaminant, as mentioned previously. Moreover, the tailorable porosity of MOFs endows the designed composites with tunable sorption selectivity and stability, which are the key factors for catalysis. Through visible light radiation, the creation of electronic / hole pairs will be caused, causing the chemical reactions necessary for catalytic activity.^[34]

With the purpose of investigate the efficiency of the different composites for removing the organic pollutants, the catalytic activity will be evaluated. The time-dependent removal of contaminants will be investigated. In order to evaluate the capacity of the different composites in both extraction and photocatalysis, comparisons for the removal of contaminants in aqueous solution will be made between synthesized composites, MOFs precursors and TiO₂ photocatalysts.

5. Conclusions

UiO-66, UiO-66-NH₂ and CIM80 metal organic frameworks and different phases of TiO₂ have been used to fabricate binary TiO₂/MOF composites. Thus, 15 new composites have been

synthesized and characterized by means of three different strategies, which can be classified into three types: (i) the formation of TiO₂ from its precursor onto as-prepared MOFs; (ii) the *in-situ* formation of TiO₂@ MOF from the organic ligand, metal template and different precursors of TiO₂ and (iii) the functionalization of titanium oxide particles with carboxylic groups prior to the growth of MOF shell around. The different synthetic factors (temperature, reaction time, etc.) have been carefully analyzed to introduce some degree of control in the preparation of the different composites and therefore, tune the morphology, crystalline phase, and composition of the different compounds.

TiO₂/MOF composites demonstrate good extraction capabilities with six different pollutants, thus indicating the immobilization of MOFs onto non-porous TiO₂ is not a disadvantage for the extraction efficiency. In general, the functionalized UiO-66-NH₂ composites have shown the best results as sorbent in a dispersive microextraction strategy. The more hydrophobic and bulky organic pollutants, 3-Benzophenone and Benzylparaben molecules, have shown the best extraction performance.

Photocatalytic activity studies to accomplish organic pollutants degradations will be performed with the different isolated TiO₂/MOF composites.

Acknowledgements

Financial support from the University of La Laguna (ULL) with the starting grant project M-ULL, with the support of the Spanish Ministry of Science, Innovation and Universities are gratefully acknowledged. We thank the SEGA services of the University of La Laguna for the access to their equipment. Patricia I. Napolitano

Tabares and Adrian Gutiérrez Serpa are acknowledged for the analytical experiments performed.

I would like to thank my tutor, Dr. Ana Lago, for her help and advice to carry out this master thesis.

I would also like to thank the members of the MAT4LL lab group for their help and the inorganics lab for allowing me to learn and work alongside them.

Finally, to my mother and my grandmother who have always been there supporting me in all my decisions.

Notes and references

- M. Petrovió, S. Gonzalez, and D. Barceló, Analysis and removal of emerging contaminants in wastewater and R. Naidu, V.A. Arias Espana, Y. Liu, J. Jit, Emerging contaminants in the environment: Risk-based analysis for better management, *TrAC Trends*, 2016, **154**, 350-357
- Daughton C.G, and Ternes T.A, Pharmaceuticals and personal care products in the environment: Agents of subtle change?, *ehp*, 1999,**107**,907-938
- P. González Hernández, Monitoring of emerging contaminants in waters using novel microextractive techniques (Tesis doctoral), 2020
- M.P.Suh, H. J. Park, T. K. Prasad, and D-W. Lim, Hydrogen storage in metal-organic frameworks, *Chem Rev.*,2012, **112**, 782-835
- Z-J. Lin, Z- Yang, T-F. Liu, Y-B. Huang, and R. Cao, Microwave-assisted synthesis of a series of lanthanide metal-organic frameworks and gas sorption properties, *Inorg. Chem.*, 2012, **51**, 1813-1820
- V. Pascanu, G. González Miera. A. Ken Inge, and B. Martín-Matute, Metal-organic frameworks as catalysts for organic synthesis: a critical perspective, *J.Am.Chem. Soc.*, 2019, **141**, 7223-7234
- X. Zhao, Y. Wang, D-S. Li, X. Bu, and P. Feng, Metal-organic frameworks for separation, *Advance Materials*, 2018, **37**, 1705189
- K.K. Tanabe, and S.M. Cohen, Postsynthetic modification of metal-organic frameworks – a progress report, *Chem. Soc. Rev.* 2011, **40**, 498-519
- J. Zhang, and Z. Chen, Metal-organic frameworks as stationary phase for application in chromatographic separation, *J Chromatogr A.*, 2017, **1530**, 1-18
- A. Gutiérrez-Serpa, A.I. Jiménez-Abizanda, F.Jiménez-Moreno, J. Pasán, and V. Pino, Core-shell microparticles formed by the metal-organic framework CIM-80(Al) (Silica@CIM-80(Al)) as sorbent material in miniaturized dispersive solid-phase extraction, *Epub*, 2020, **211**, 120-723
- I. Taima-Macera, P. Rocío-Bautista, J. Pasán, J.H. Ayala, C. Ruiz-Pérez, A.M. Afonso, A. B. Lago, and V. Pino, Influence of ligand functionalization of UiO-66-Based metal-organic frameworks when used as sorbents in dispersive solid-phase analytical microextraction for different aqueous organic pollutants, *Molecules*, 2018, **23**, 2869
- Q.Yang, S. Vaesen, F. Ragon, A. Wiersum, D. Wu, A. Lago, T. Devic, C. Martineau, F. Taulelle, P. L. Llewellyn, et al. A water stable metal-organic framework with optimal feature for CO₂ capture, *Angew. Chem.-Int. Edit.*,2013, **52**, 10316-10320
- Y. Cao, X. Chen, X. Li, and B. Wang, Tuning surface functionalization and pore structure of UiO-66 metal-organic framework nanoparticles for organic pollutant elimination, *ACS Appl. Nano Mater*, 2021, **4**, 5, 5486-5495
- M. Kandiah, M. Hellner Nilsen, S. Usseglio, S. Jakobsen, U. Olsbye, M. Tilset, C. Larabi, E. A. Quadrelli, F. Bonino, and K. P. Lillerud, Synthesis and stability of tagged UiO-66 Zr-MOFs, *Chem. Matter.* 2010, **22**,24, 6632-6640
- Z. H. Rada, H. R. Abid, H. Sun, J. Shang, J. Li, Y. He, S. Liu, and S. Wang, Effects of -NO₂ and -NH₂ functional groups in mixed-linker Zr-based MOFs on gas adsorption of CO₂ and CH₄, *Progress in Natural Science*,2018, **28**, 160-167
- P. Rocío-Bautista, V. Pino, J.H. Ayala, C. Ruiz-Pérez, O. Vallcorba, A. M. Afonso, and J. Pasán, A green metal-organic framework to monitor water contaminants, *RSC Adv.*,2018, **8**, 31304
- D.E. Newbury, and N. W. M. Ritchie, Elemental mapping of microstructures by scanning electron microscopy-energy dispersive X-ray spectrometry (SEM-EDS): extraordinary advance with the silicon drift detector (SDD), *J. Anal. At. Spectrom.* 2013, **28**, 973-988
- S.E. Braslavsky, *Pure Appl. Chem.*, 2007, **79**, 293-465
- J.M. Herrmann, Destrucción de contaminantes orgánicos por fotocatalisis heterogénea, **10**, 153-170
- Yifan Gu, Yi-nan Wu, J. Shen, Z.Li, S. Chen, H. Lu, and F.Li, Turning redundant ligands into treasure: A new strategy for constructing MIL-53(Al)@Nanoscale TiO₂ layers, *Chem.*, 2015, **21**, 17485-17490
- L. Fernández-Velasco, and C. O. Ania, Materiales de carbono en fotocatalisis, 2011, **21**
- L. Fernández Velasco, Fotodegradación oxidativa de fenol con catalizadores TiO₂-C. Análisis de la respuesta fotoquímica de la fase carbonosa (Tesis doctoral), 2012
- C-C. Wang, X. Wang, and W. Liu, The synthesis strategies, and photocatalytic performances of TiO₂/MOFs composites: A state-of-the-art review, *Chem. Engineering Journal*, 2020, **391**, 123601
- M.J. Katz, Z.J. Brown, Y.J. Colón, P.W. Siu, K.A. Scheidt, R.Q. Snurr, J.T. Hupp, and O.K. Farha, A facile synthesis of UiO-66, UiO-67 and their derivatives, *Chem. Comm*, 2013, **49**, 9449-9451
- N. Chang, H. Zhang, M-S. Shi, J. Li, W. Shao, and H-T- Wang, Metal-organic framework templated synthesis of TiO₂@MIL-101 core-shell architectures for high-efficiency adsorption and photocatalysis, *Mat. Let.*, 2017, **200**, 55-58
- L. Wang, P. Jin, S. Duan, H. She, J. Huang, and Q. Wang, In-situ incorporation of Copper (II) porphyrin functionalized zirconium MOF and TiO₂ for efficient photocatalytic CO₂ reduction, *Science bulletin*, 2019, **64**, 926-933
- X. He, H. Fang, D. J. Gosztola, Z. Jiang, P. Jena, and W. Wang, Mechanistic insight into photocatalytic pathways of MIL-100(Fe)/TiO₂ composites, *ACS Appl. Mater. Interfaces* 2019, **11**,13, 12516-12524
- H. Sheng, D. Chen, N. Li, Q. Xu, H. Li, J. He, and J. Lu, Urchin-inspired TiO₂@MIL-101 double-shell hollow particles: adsorption and highly efficient photocatalytic degradation of hydrogen sulfide, *Chem Mater.*, 2017, **29**,13, 5612-5616
- M. Zhang, Q. Shang, Y. Wan, Q. Cheng, G. Liao, and Z. Pan, Self-template synthesis of double-shell TiO₂@ZIF-8 hollow nanospheres via sonocrystallization with enhanced photocatalytic activities in hydrogen generation, *Applied catalysis B: Environmental*, 2019, **241**, 149-158
- P. González Hernández, A. B. Lago, J. Pasán, C. Ruiz Perez, J.H. Ayala, A. M. Afonso, and V. Pino, Application of a pillared-layer Zn-Triazolate metal organic framework in the dispersive miniaturized solid-phase extraction of personal care products from wastewater samples, *Molecules*, 2019, **24**, 690
- R. Facorro-Souto, Use of high resolution mass/mass spectrometry for the investigation of food safety and environmental impact of organic emerging contaminants (Thesis Doctoral), 2021
- A. Nandy, A. C. Forse, V. J. Witherspoon, and J. A. Reimer, NMR spectroscopy reveals adsorbate binding sites in the metal-organic framework UiO-66(Zr), *J. Phys. Chem. C*, 2018,**122**,15, 8295-8305
- S. Dai, A. Tissot, and C. Serre, Recent progresses in metal-organic frameworks based core-shell composites, *Adv. E. Mat.*,2021.
- Y. Li, J. Jiang, Y. Fang, Z. Cao, D. Chen, N. Li, Q. Xu, and J. Lu, TiO₂ nanoparticles anchored onto the metal-organic framework NH₂-MIL-88B(Fe) as an adsorptive photocatalyst with enhanced fenton-like degradation of organic pollutants under visible light irradiation, *ACS Sus. Chem. Eng.*, 2018, **6** (12), 16186-16197

Supplementary Material

Facultad de
Ciencias –
Universidad de la
Laguna.

Master in
Molecular
Nanoscience and
Nanotechnology

Course 2020-2021

Materials based on metal organic frameworks for the removal of emerging pollutants in water

Yaiza Martín García

Supervisor: Ana Belén Lago Blanco

Laboratorio de Materiales para Análisis Químicos (MAT4LL), Departamento de Química, Unidad
Departamental de Química Inorgánica, Universidad de La Laguna (ULL), La Laguna, Tenerife, 38206, Spain.

Contents:	Pag.
INTRODUCCION	3
Table S1. Name, structure, and water solubility of the different analytes	
Fig S1a. UiO-66 structure. Metal and ligand precursors	
Fig S1b. UiO-66-NH ₂ structure. Metal and ligand precursors	4
Fig S1c. CIM-80 structure. Metal and ligand precursors	
Table S2. Name, MOF and TiO ₂ used for the composite and the synthetic procedures	5
Fig S2a. Scheme of the synthesis for 1 - 6 composites	6
Fig S2b. Scheme of the synthesis for 7 - 12 composites	
Fig S2c. Scheme of the synthesis for 13 - 15 composites	7
CHARACTERIZATION OF MOFs	
Fig S3. The scheme of the fabrication and synthesis of 1-15 composites	
Fig S4. Core @ shell structure for the raised method: (a) MOF @ TiO ₂ and (b) TiO ₂ @ MOF	8
<i>X-ray powder diffractograms</i>	
Fig S5a. X-Ray powder diffractogram of UiO-66 and UiO-66-NH ₂	
Fig S5b. X-Ray powder diffractogram of CIM-80	9
<i>Study of structural transformation</i>	10-11
Fig S6a. IR spectra of MOF UiO-66	
Fig S6b. IR spectra of MOF UiO-66-NH ₂	
Fig S6c. IR spectra of MOF CIM-80	
CHARACTERIZATION OF COMPOSITES	12-14
Universidad de La Laguna. Máster en Nanociencia y Nanotecnología Molecular.	1

MOF @ TiO₂ (30% and 50%) composites*X-ray powder diffractograms*

Fig S7a. X-Ray powder diffractogram of **1**, and **2** composites

Fig S7b. X-Ray powder diffractogram of **4**, and **5** composites

Fig S7c. X-Ray powder diffractogram of **3**, and **6** composites

Thermogravimetric analysis

15-16

Fig S8a. TGA of **1**, **2**, and **3** composites

Fig S8b. TGA of **4**, **5**, and **6** composites

Study of structure

Table S3. BET surfaces area, particle size and % MOF/TiO₂ for **1-6** composites

TiO₂ @ MOF composites. In-situ approach

17-18

X-Ray powder diffractograms

17-18

Fig S9a. X-Ray powder diffractogram of **7 - 9** composites

Fig S9b. X-Ray powder diffractogram of **10 - 12** composites

Thermogravimetric analysis

19-20

Fig 10a. TGA of **7 - 9** composites

Fig 10b. TGA of **10 - 12** composites

Study of structure

Table S4. Particle size for **6-12** composites

TiO₂ @ MOF composites. Functionalized process

21

Fig S11. FT-IR spectrum of functionalized titanium oxide particle

Fig S12. X-Ray powder diffractogram for **13**, and **14** composites

22

Fig S13. FT- IR spectrum for (a) **13**, (b) **14** and (c) **15** composites

23-24

Study of morphology

25

Fig S14. (a) SEM of CIM-80 @ TiO₂ (30%) and elemental mapping of composite (b) aluminium, (c) titanium, (d) oxygen.

ADSOPTION ANALYTES

26

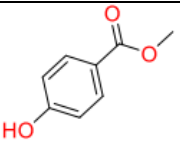
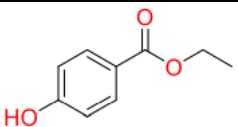
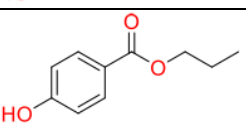
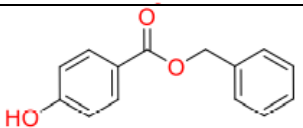
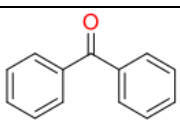
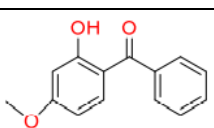
Fig S15. Comparison between the different composites and precursors used in terms of extraction efficiency for each analyte

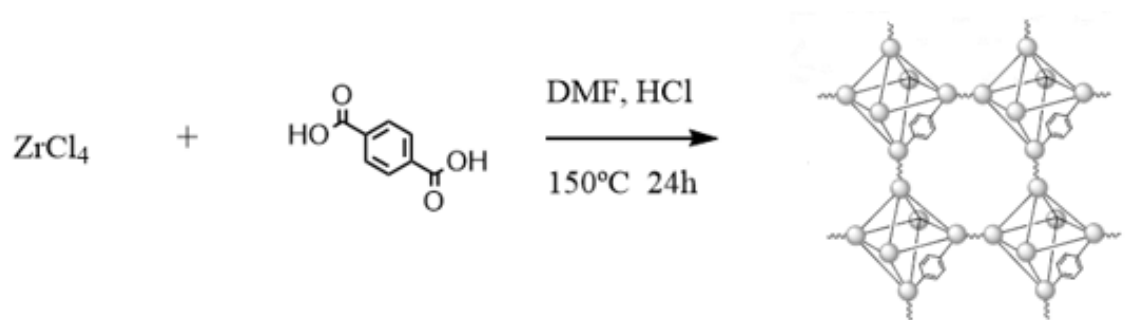
Table S5. Same of main analytical parameters of chromatographic methods.

27

INTRODUCTION

Table S1. Name, structure, and water solubility of the different analytes

Analyte (abbreviation)	Structure	Water solubility (g/L) (25°C)
Methylparaben (MPB)		2.5
Ethylparaben (EPB)		2.5
Propylparaben (PPB)		2.5
Benzylparaben (BzPB)		2.5
Benzophenone (BP)		Insoluble
3-Benzophenone (3-BP)		Insoluble

**Fig S1a.** UiO-66 structure. Metal and ligand precursors

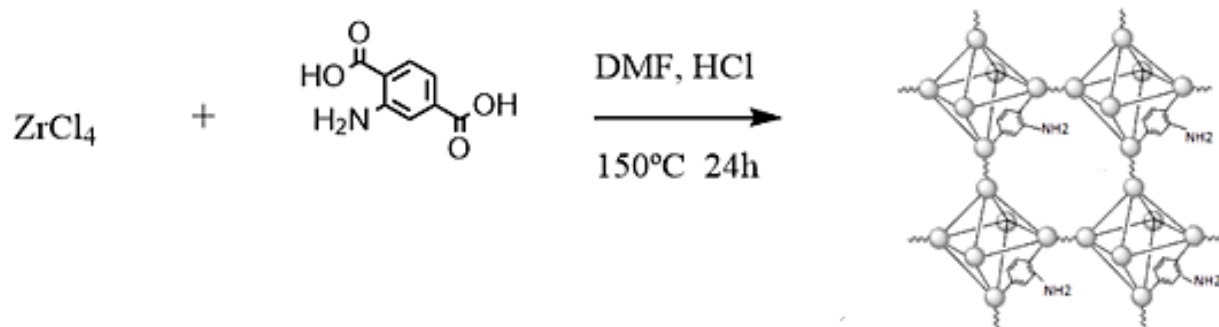


Fig S1b. UiO-66-NH₂ MOF structure. Metal and ligand precursors

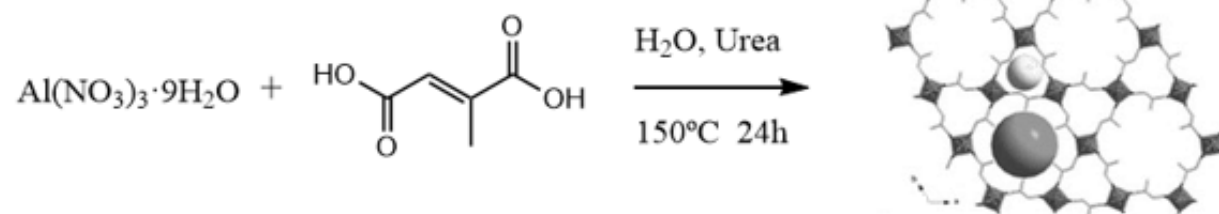


Fig S1c. CIM-80 MOF structure. Metal and ligand precursors.

Table S2. Name, MOF and TiO₂ used for the composite and the synthetic procedures.

Composite Photocatalysts	MOF	TiO ₂
UiO-66 @ TiO ₂ (30%) (1)	UiO-66 (Zr)	TBT*
UiO-66-NH ₂ @ TiO ₂ (30%) (2)	UiO-66-NH ₂ (Zr)	TBT
CIM-80 @ TiO ₂ (30%) (3)	CIM-80 (Al)	TBT
UiO-66 @ TiO ₂ (50%) (4)	UiO-66 (Zr)	TBT
UiO-66-NH ₂ @ TiO ₂ (50%) (5)	UiO-66-NH ₂ (Zr)	TBT
CIM-80 @ TiO ₂ (50%) (6)	CIM-80 (Al)	TBT
Ultrasound treatment and hydrothermal method were adopted to prepare 1-6 with UiO-66, UiO66-NH ₂ , CIM-80 and tetrabutyl titanate as precursors a		
P21 @ UiO-66 (7)	UiO-66 (Zr)	P21**
One-step hydrothermal method was adopted to prepare P21 @ UiO66 with ZrCl ₄ , titanium (IV) oxide anatase, and amino-terephthalic acid as precursors.		
P25 @ UiO-66 (8)	UiO-66 (Zr)	P25**
One-step hydrothermal method was adopted to prepare P25 @ UiO66 with ZrCl ₄ , titanium (IV) oxide (P25), and amino-terephthalic acid as precursors.		
P100 @ UiO-66 (9)	UiO-66 (Zr)	P100**
One-step hydrothermal method was adopted to prepare P100 @ UiO66 with ZrCl ₄ , titanium (IV) oxide mixture of rutile and anatase, and amino-terephthalic acid as precursors.		
P21 @ UiO-66-NH ₂ (10)	UiO-66-NH ₂ (Zr)	P21
One-step hydrothermal method was adopted to prepare P21 @ UiO66-NH ₂ with ZrCl ₄ , titanium (IV) oxide anatase, and 2- amino-terephthalic acid as precursors.		
P25 @ UiO-66-NH ₂ (11)	UiO-66-NH ₂ (Zr)	P25
One-step hydrothermal method was adopted to prepare P25 @ UiO66-NH ₂ with ZrCl ₄ , titanium (IV) oxide (P25), and 2- amino-terephthalic acid as precursors.		
P100 @ UiO-66-NH ₂ (12)	UiO-66-NH ₂ (Zr)	P100
One-step hydrothermal method was adopted to prepare P100 @ UiO66-NH ₂ with ZrCl ₄ , titanium (IV) oxide mixture of rutile and anatase, and 2- amino-terephthalic acid as precursors.		
TiO ₂ -COO @ UiO-66 (13)	UiO-66	P25
TiO ₂ -COO @ UiO-66-NH ₂ (14)	UiO-66-NH ₂	P25
The mixture prepared with the TiO ₂ particles functionalized with the carboxyl group and MOF building block was heated at 80 °C for 24 h.		
TiO ₂ -COO @ CIM-80 (15)	CIM-80 (Al)	P25
The mixture prepared with the TiO ₂ particles functionalized with the carboxyl group, Al (NO ₃) ₃ ·9H ₂ O, mesaconic acid, urea and H ₂ O was heated at 150 °C for 24 h.		

*TBT = tetrabutyl titanate.

**P25 = titanium oxide particles (mixed phases, size 21 nm); P21 = titanium oxide particles (pure phase, size <25 nm); P100 = titanium oxide particles (mixed phases, size 100 nm)

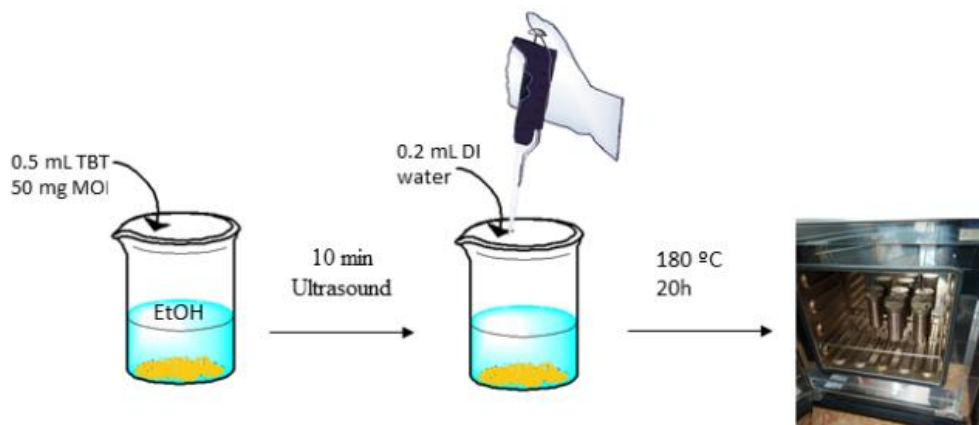


Fig S2a. Scheme of the synthetic procedure followed for the synthesis of **UiO-66 @ TiO₂ (30%) (1)**; **UiO-66-NH₂ @ TiO₂ (30%) (2)**; **CIM-80 @ TiO₂ (30%) (3)**; **UiO-66 @ TiO₂ (50%) (4)**; **UiO-66-NH₂ @ TiO₂ (50%) (5)** and **CIM-80 @ TiO₂ (50%) (6)** composites

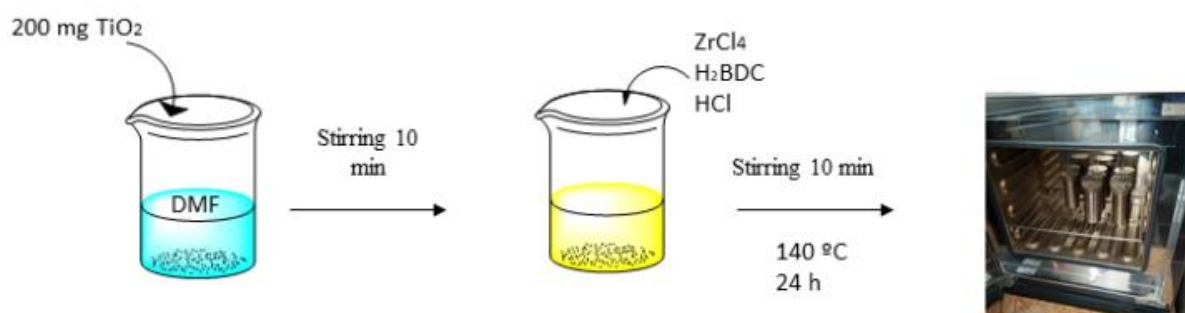


Fig S2b. Scheme of the synthetic procedure followed for **P21 @ UiO-66 (7)**; **P25 @ UiO-66 (8)**; **P100 @ UiO-66 (9)**; **P21 @ UiO-66-NH₂ (10)**; **P25 @ UiO-66-NH₂ (11)**; **P100 @ UiO-66-NH₂ (12)** composites

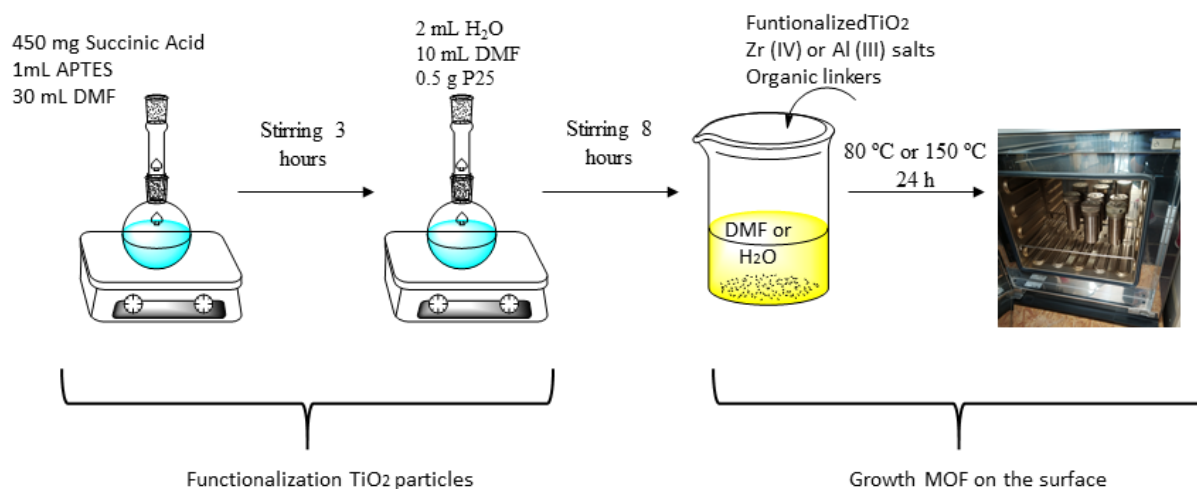


Fig S2c. Scheme of the synthetic procedure followed for **TiO₂-COO @ UiO-66 (13)**; **TiO₂-COO @ UiO-66-NH₂ (14)**; **TiO₂-COO @ CIM-80 (15)** composites

CHARACTERIZATION OF MOFs



Fig S3. The scheme of the fabrication and synthesis of **1-15** composites

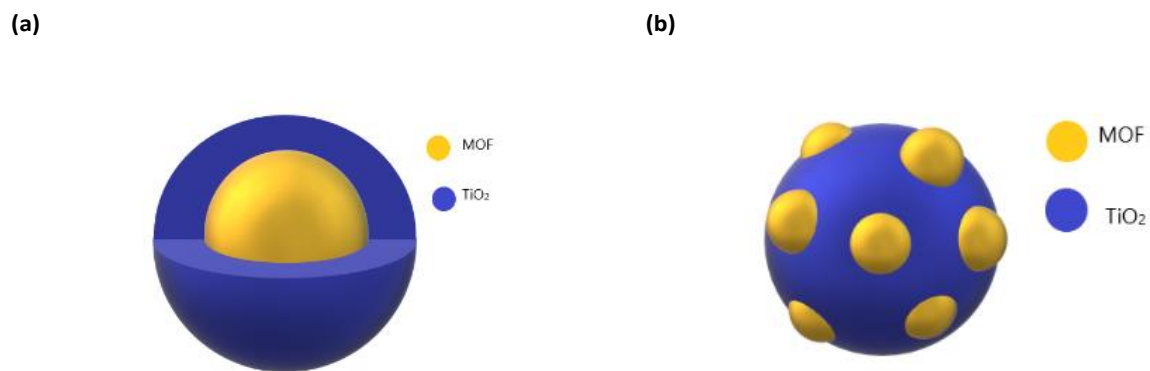


Fig S4. Core-shell structure for the raised methods: (a) MOF @ TiO₂ and (b) TiO₂ @ MOF

X-ray powder diffractograms

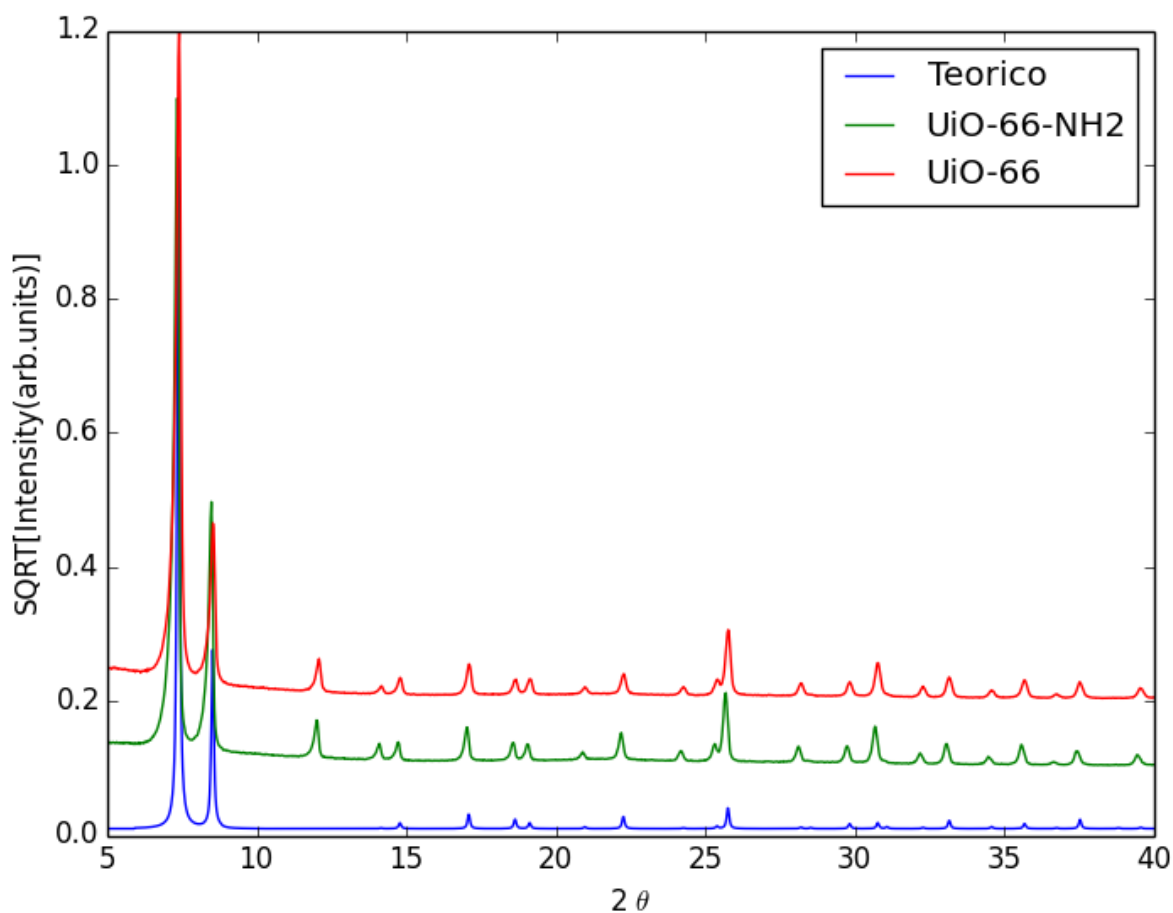


Fig S5a. X-Ray powder diffractogram of UiO-66 and UiO-66-NH₂

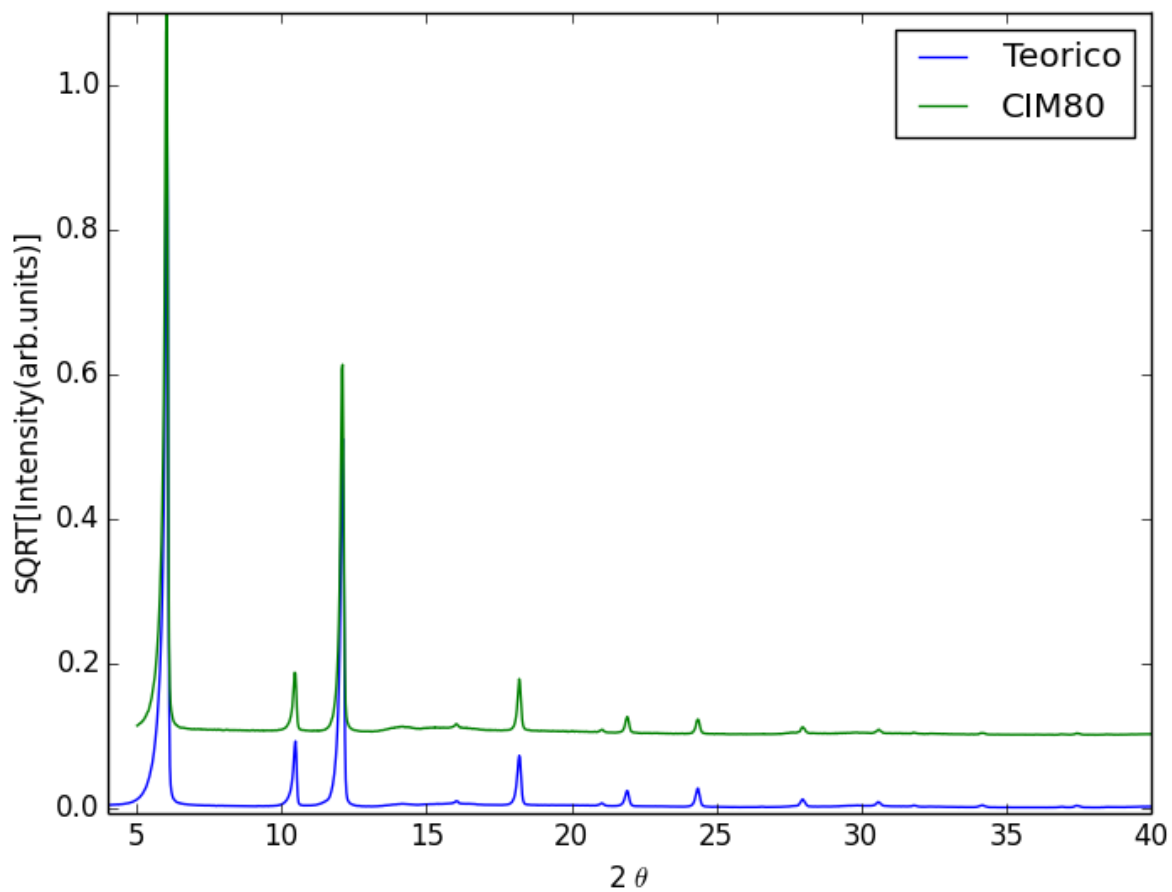


Fig S5b. X-Ray powder diffractogram of CIM-80

Study of structural transformation

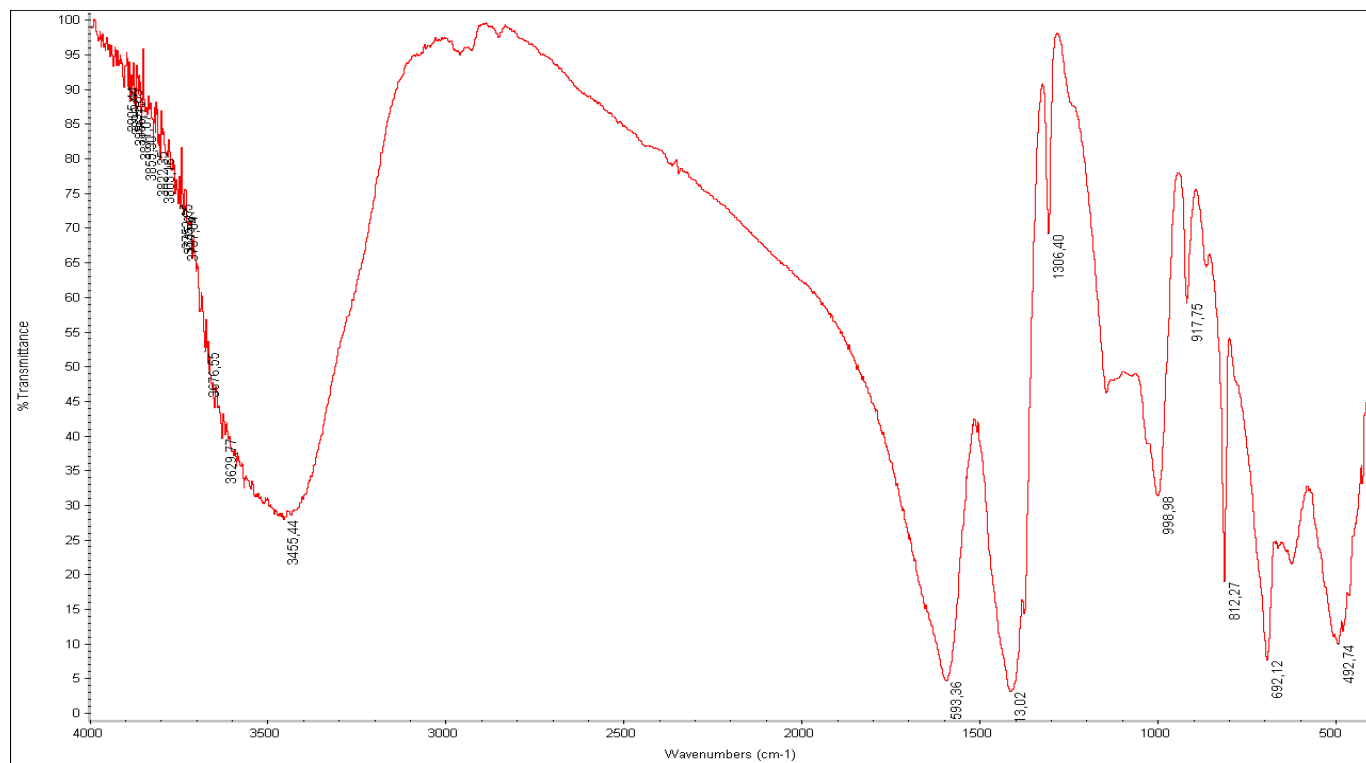
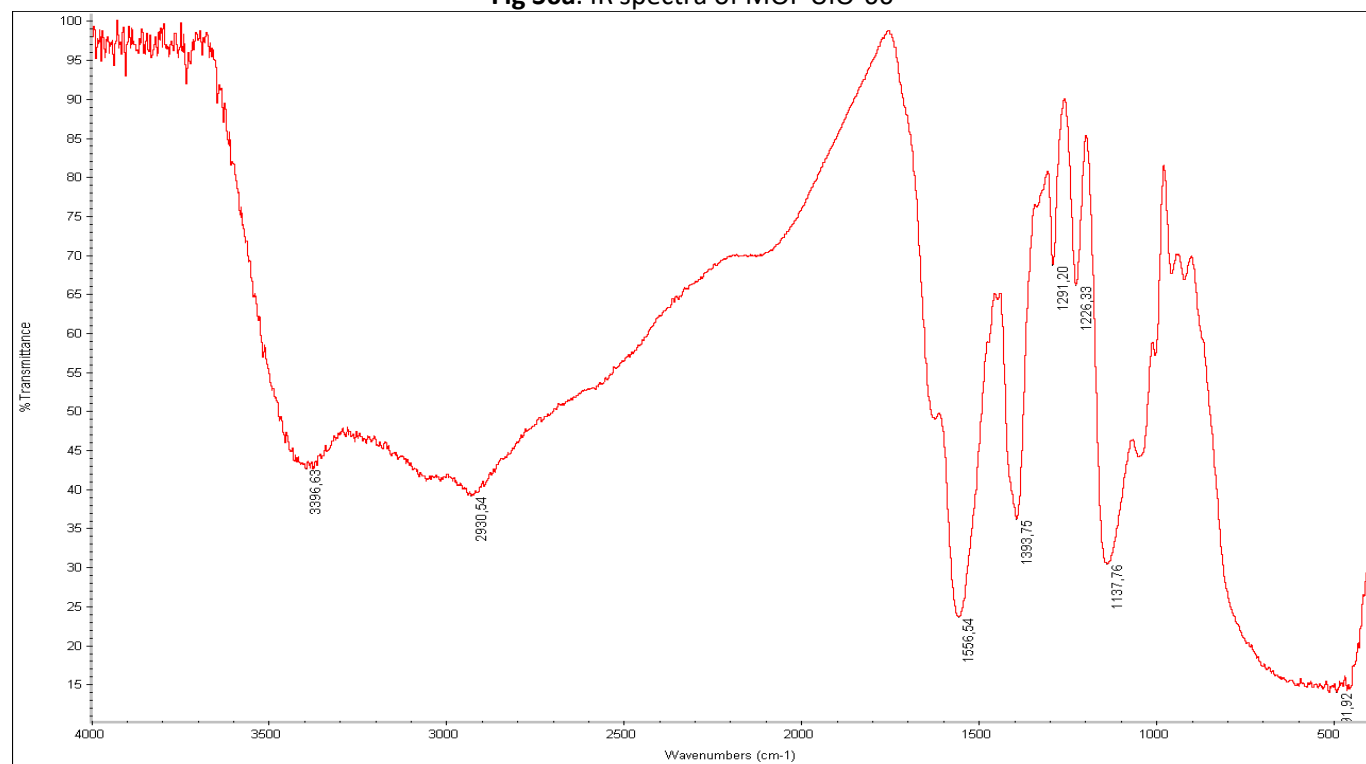


Fig S6a. IR spectra of MOF UiO-66

Fig S6b. IR spectra of MOF UiO-66-NH₂

CHARACTERIZATION OF COMPOSITES

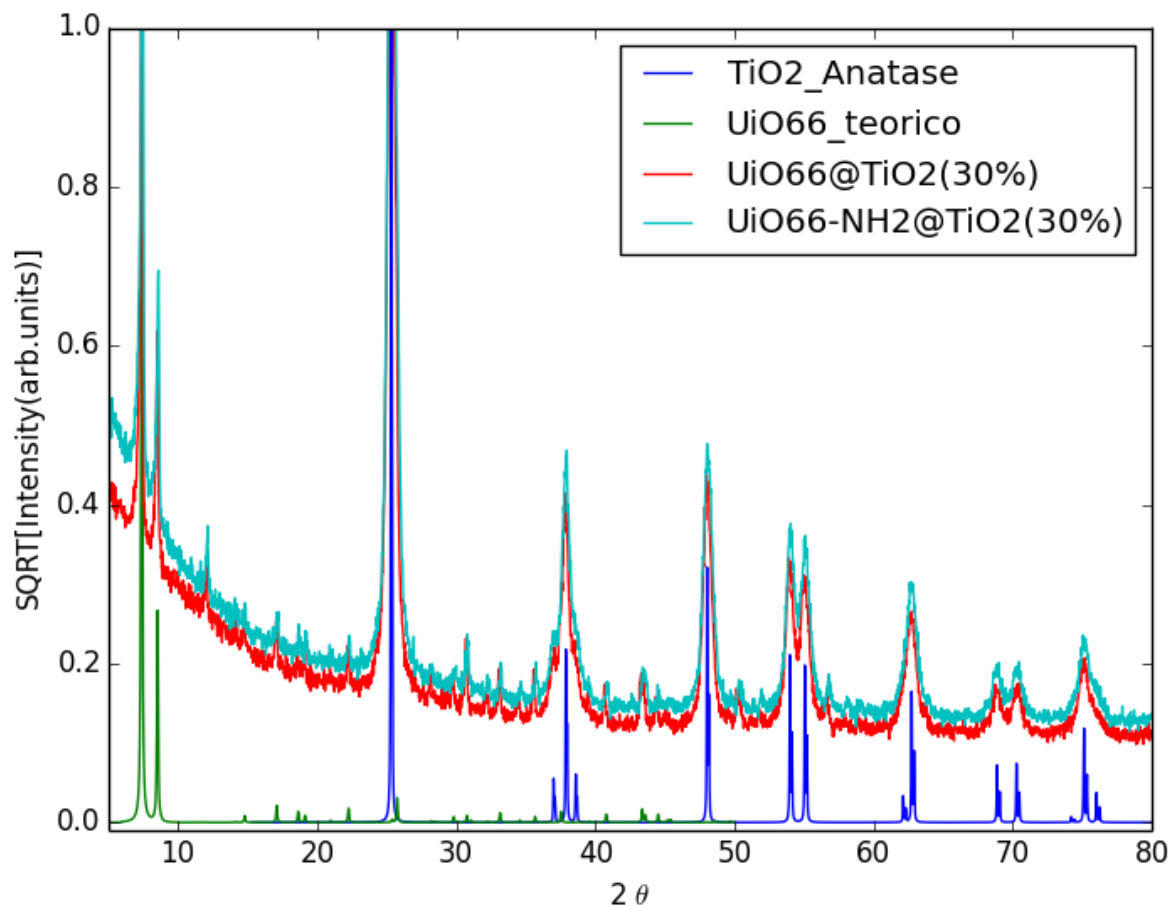
MOF @ TiO₂ (30% and 50%) composites*X-ray powder diffractograms*

Fig S7a. X-Ray powder diffractogram of **UiO-66 @ TiO₂(30%) (1)** and **UiO-66-NH₂ @ TiO₂(30%) (2)**

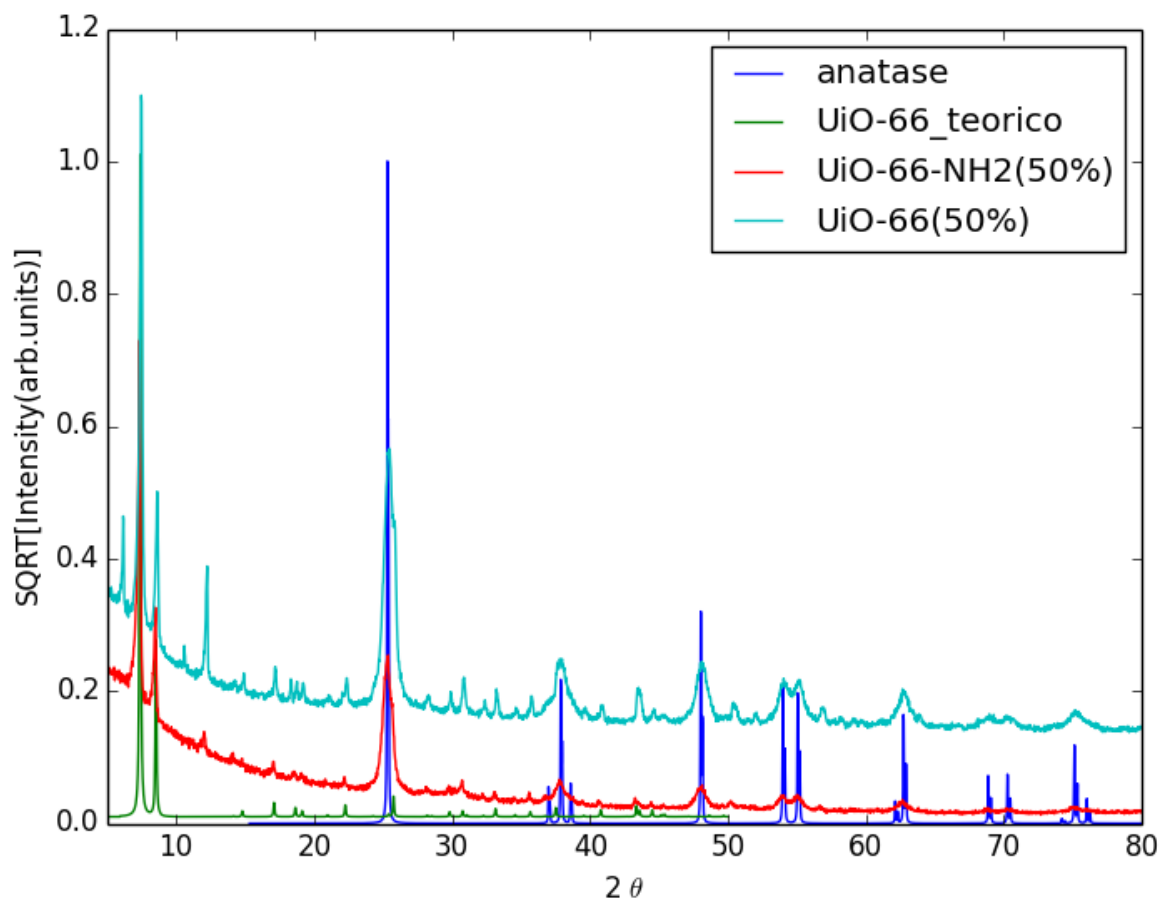


Fig S7b. X-Ray powder diffractogram of UiO-66 @ TiO₂(50%) (4) and UiO-66-NH₂ @ TiO₂(50%) (5)

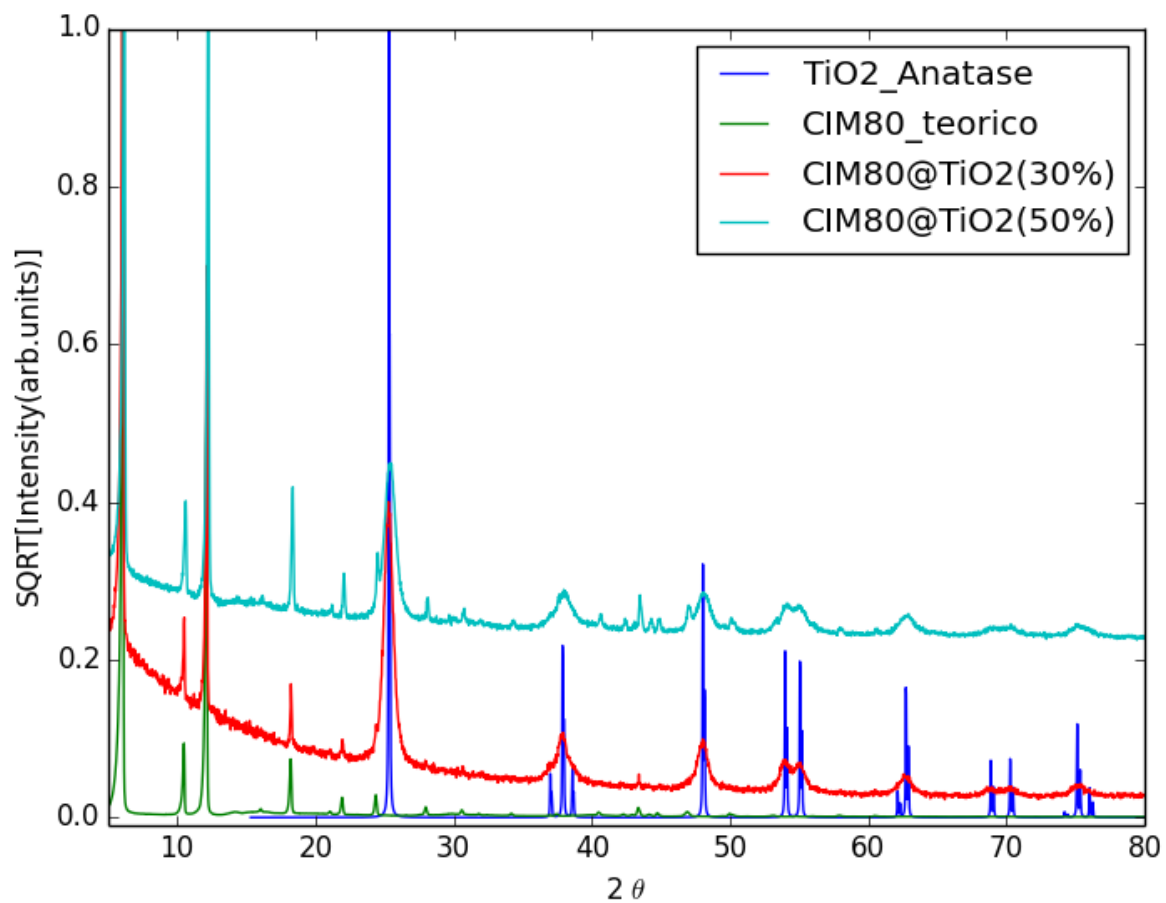


Fig S7c. X-Ray powder diffractogram of **CIM-80 @ TiO₂(30%) (3)** and **CIM-80 @ TiO₂(50%) (6)**

Thermogravimetric analysis

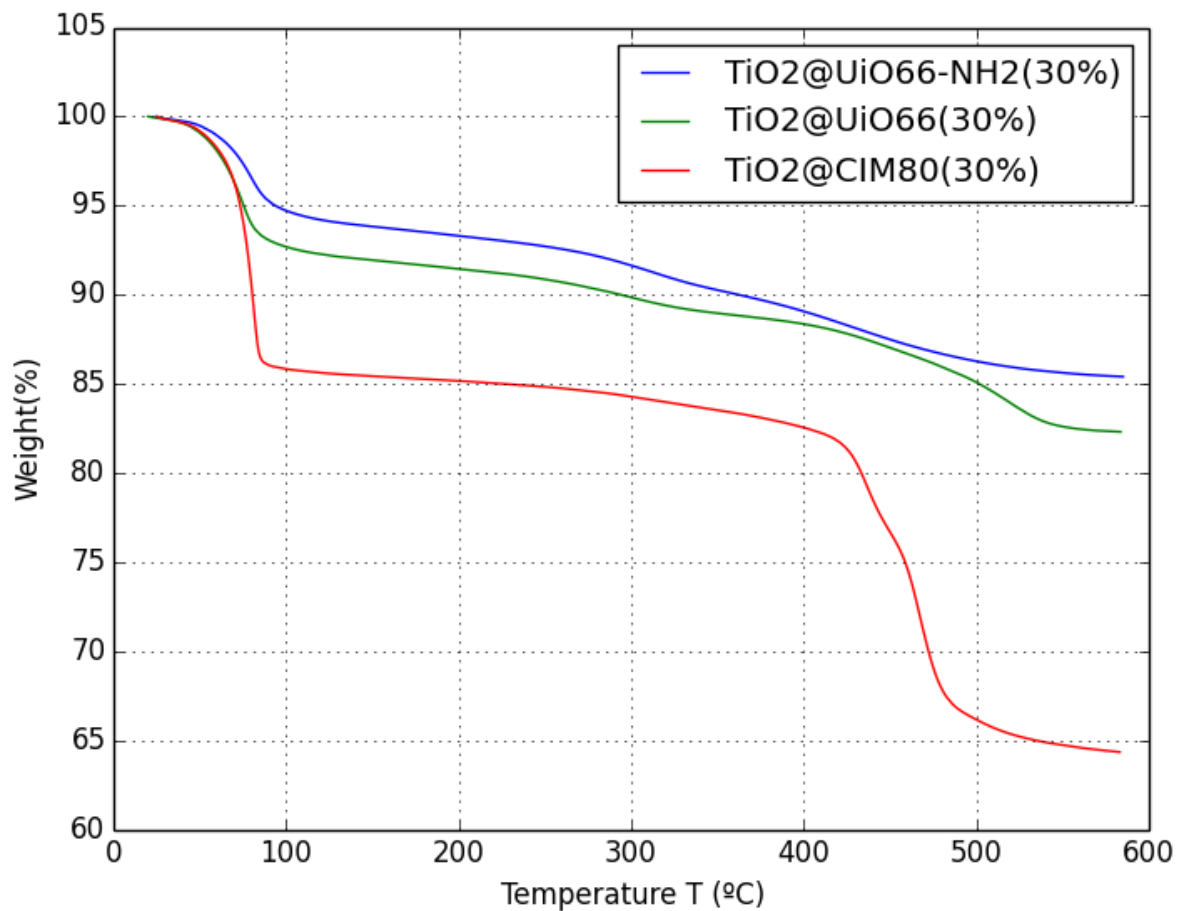


Fig S8a. TGA of TiO₂ @ UiO-66 (30%) (1), TiO₂ @ UiO-66 - NH₂ (30%) (2), TiO₂ @ CIM-80(30%) (3) composites

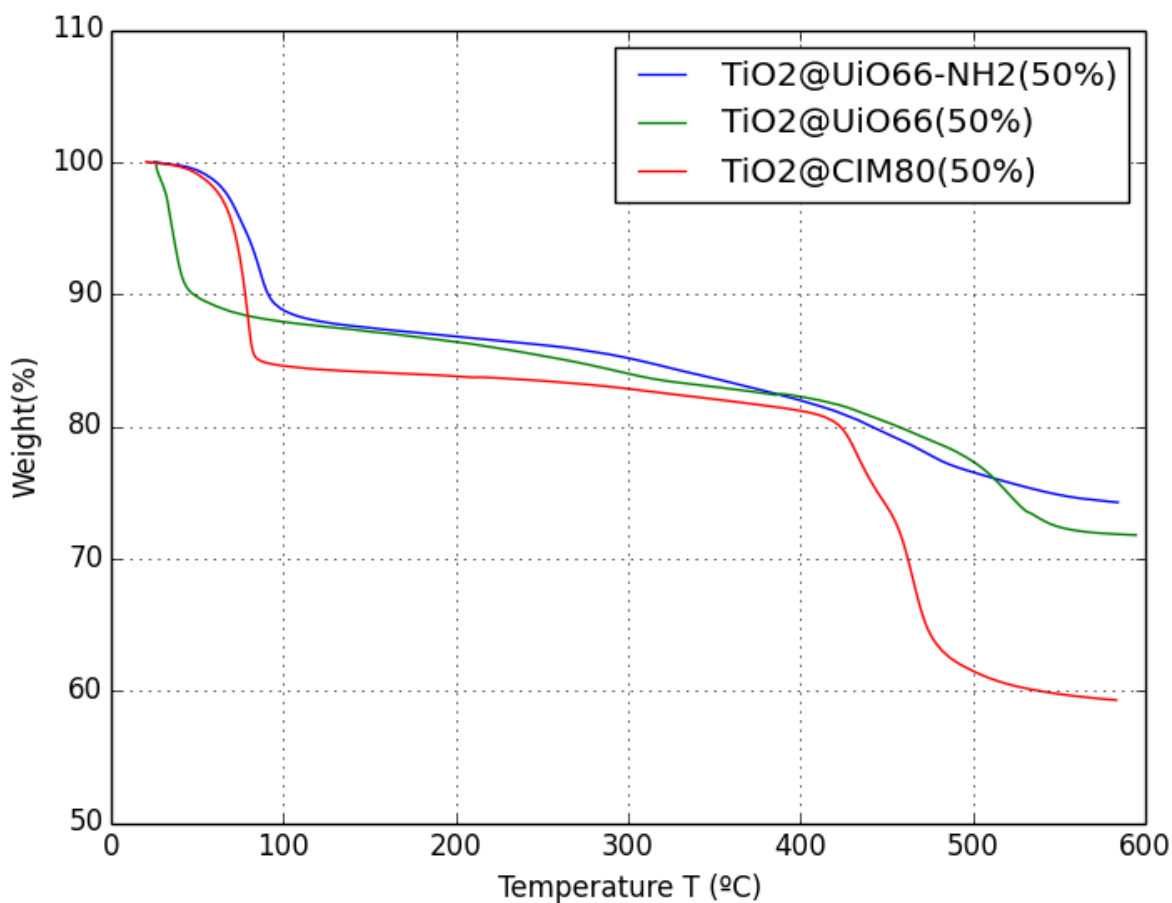


Fig S8b. TGA of TiO₂ @ UiO-66 (50%) (4), TiO₂ @ UiO-66-NH₂ (50%) (5), TiO₂ @ CIM-80 (50%) (6) composites

Study of structure

Table S3. BET surface area, particle size and % MOF/TiO₂ for UiO-66 @ TiO₂ (30%) (1); UiO-66-NH₂ @ TiO₂ (30%) (2); CIM-80 @ TiO₂ (30%) (3); UiO-66 @ TiO₂ (50%) (4); UiO-66-NH₂ @ TiO₂ (50%) (5) and CIM-80 @ TiO₂ (50%) (6)

MOF – TiO ₂	BET Surface area (m ² /g)	Particle size (nm)
UiO-66 @ TiO ₂ (30%) (1)	276	1000
UiO-66-NH ₂ @ TiO ₂ (30%) (2)	275	4062
CIM-80 @ TiO ₂ (30%) (3)	2	1000
UiO-66 @ TiO ₂ (50%) (4)	429	948
UiO-66-NH ₂ @ TiO ₂ (50%) (5)	.*	309
CIM-80 @ TiO ₂ (50%) (6)	643	143

*Compound 5 has not been characterized by N₂ adsorption

TiO₂ @ MOF composites. In-situ approach

X-Ray powder diffractograms

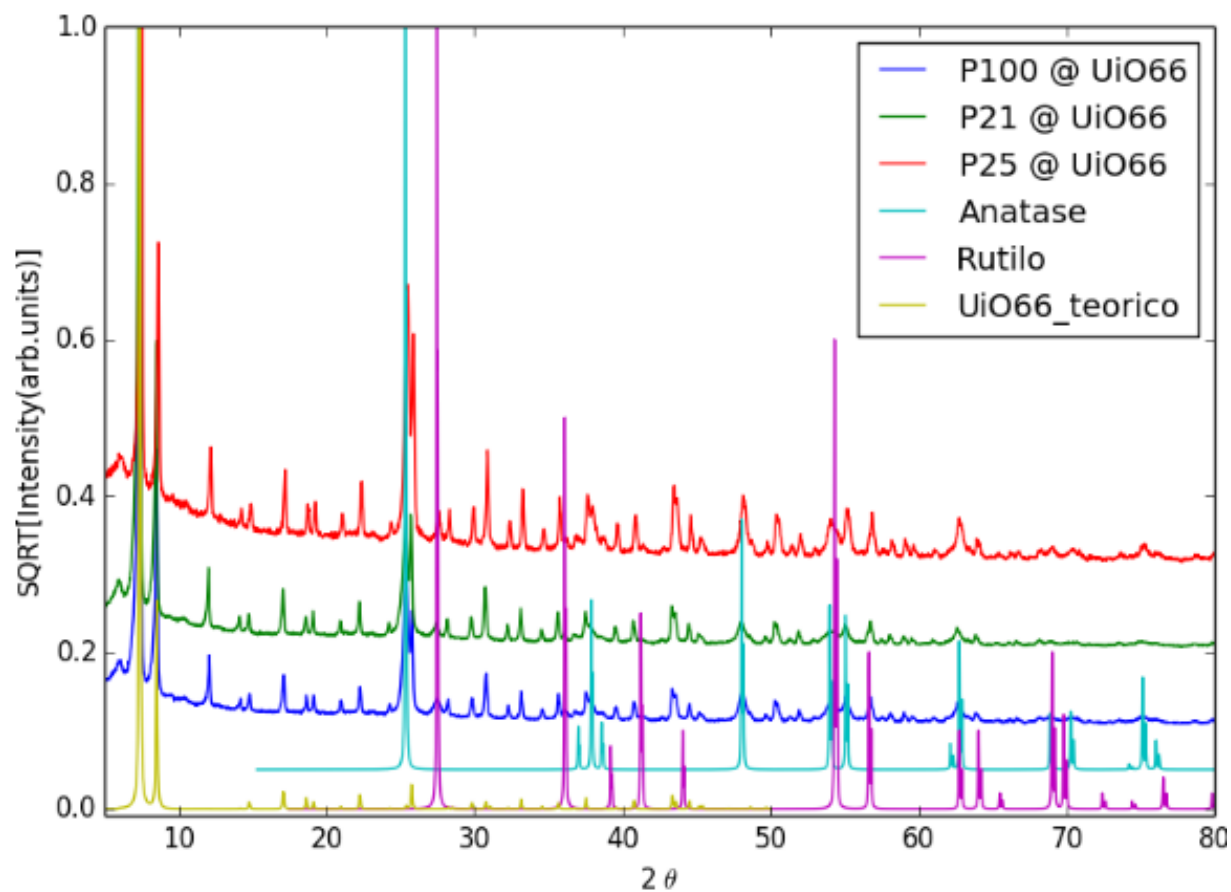


Fig S9a. X-ray powder diffractogram of P21 @ UiO-66 (7); P25 @ UiO-66 (8); P100 @ UiO-66 (9) composites

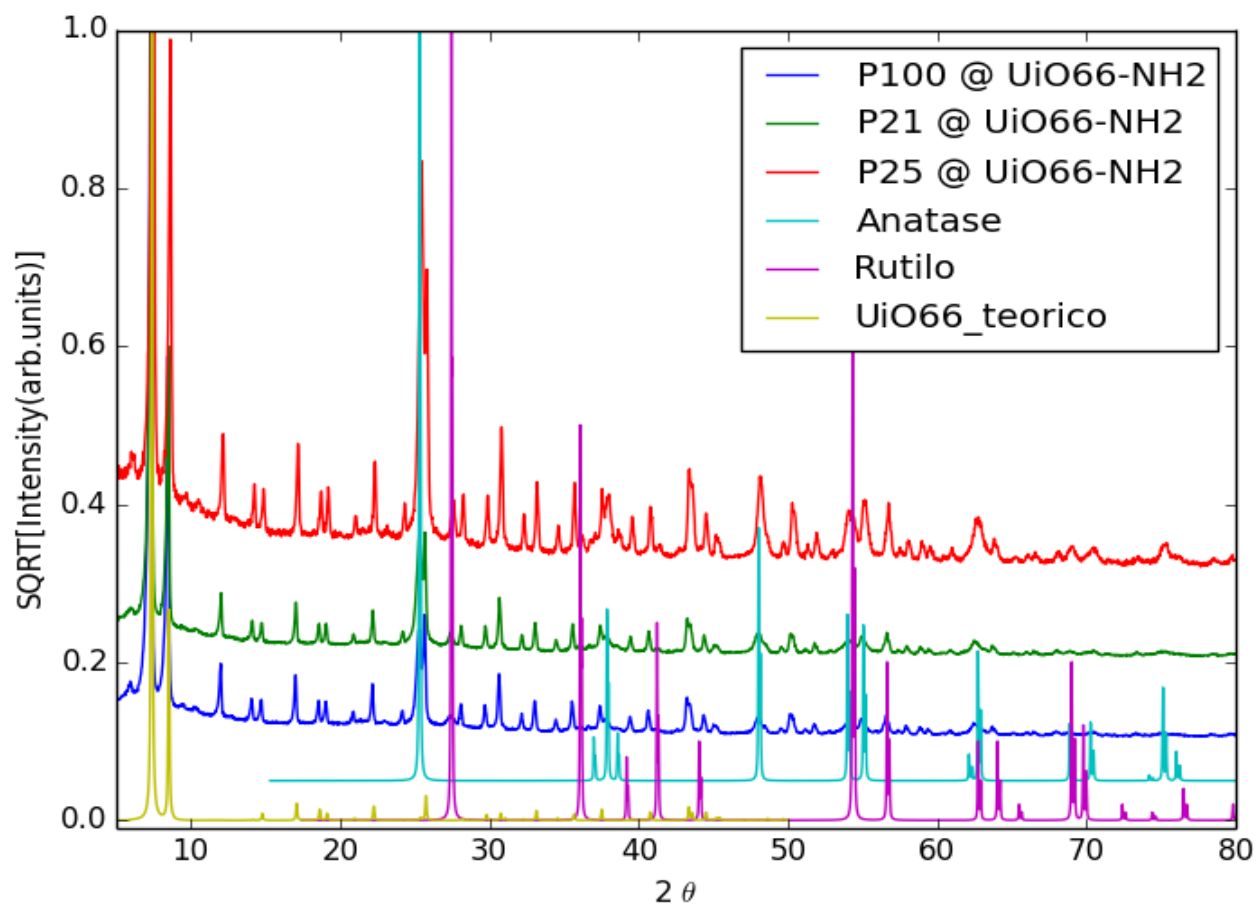


Fig S9b. X-ray powder diffractogram of **P21 @ UiO-66-NH₂ (10)**; **P25 @ UiO-66-NH₂ (11)**; **P100 @ UiO-66-NH₂ (12)** composites

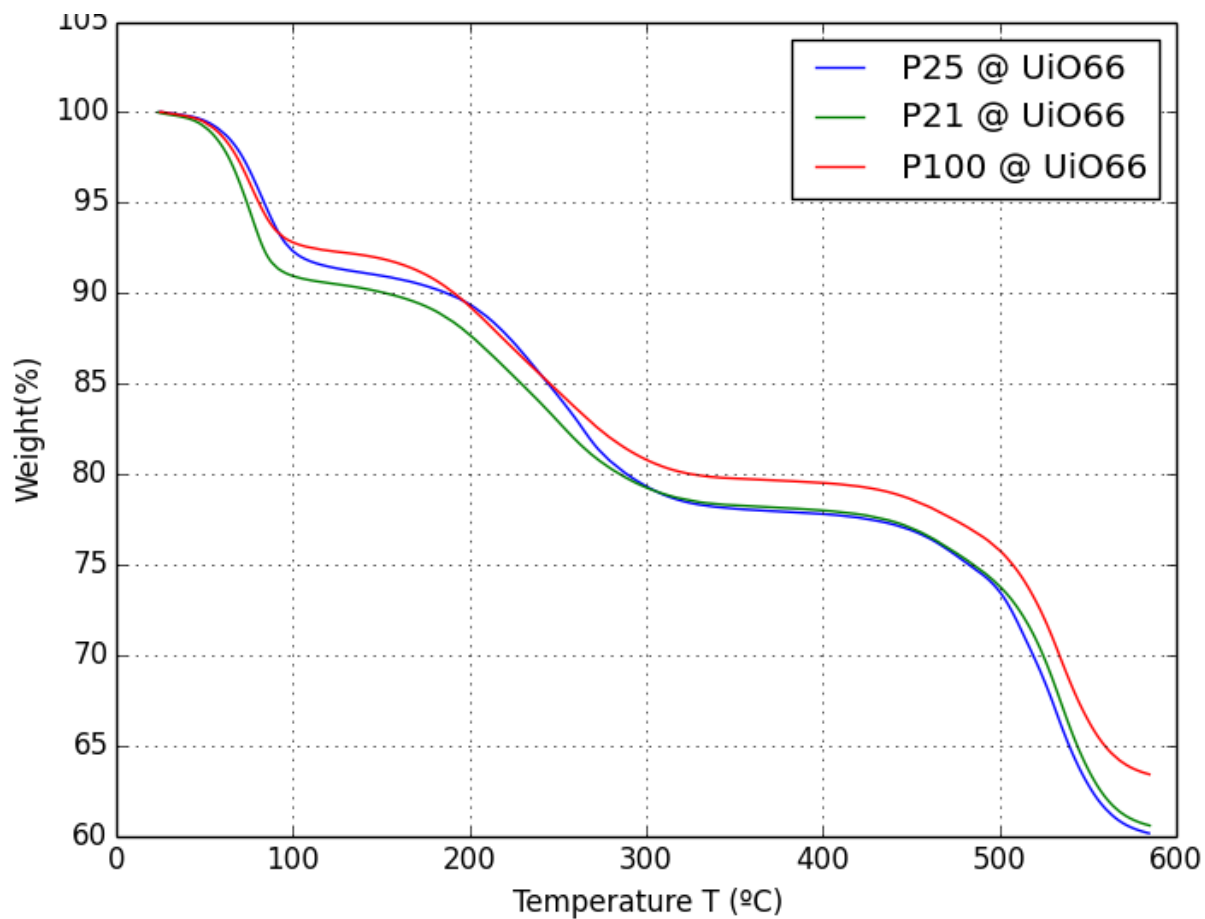
Thermogravimetric analysis

Fig S10a. TGA of P21 @ UiO-66 (7); P25 @ UiO-66 (8); P100 @ UiO-66 (9) composites

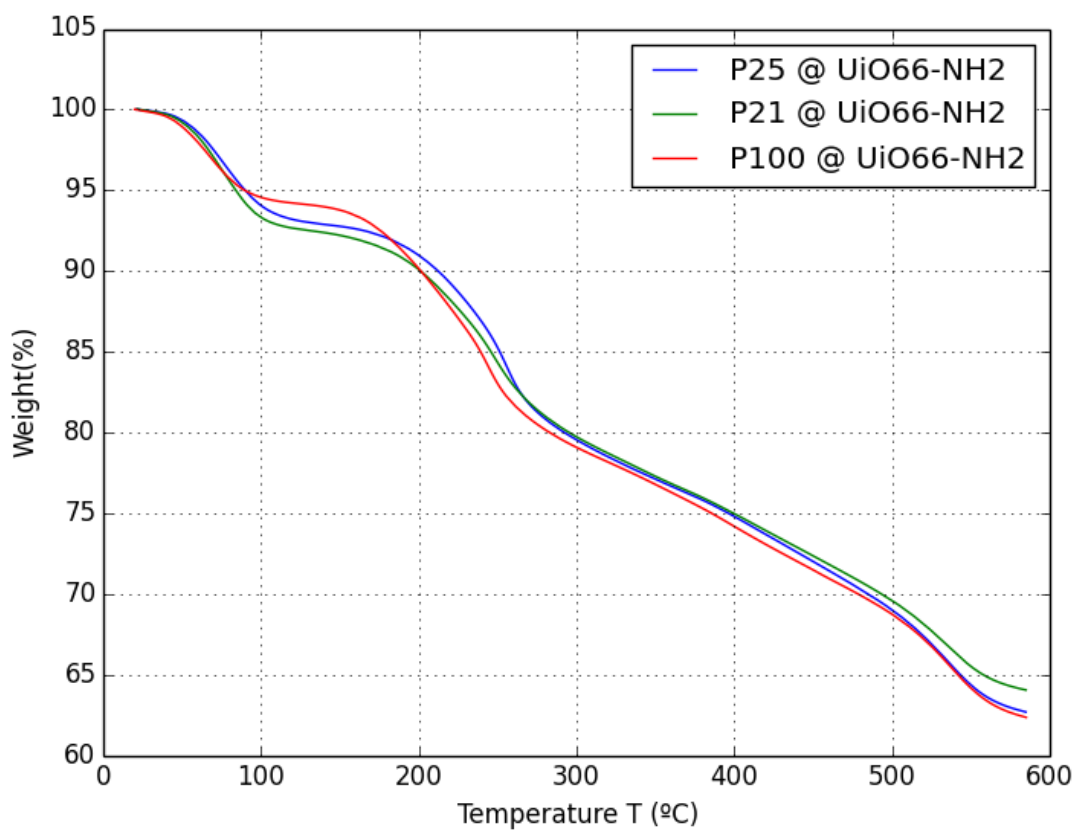
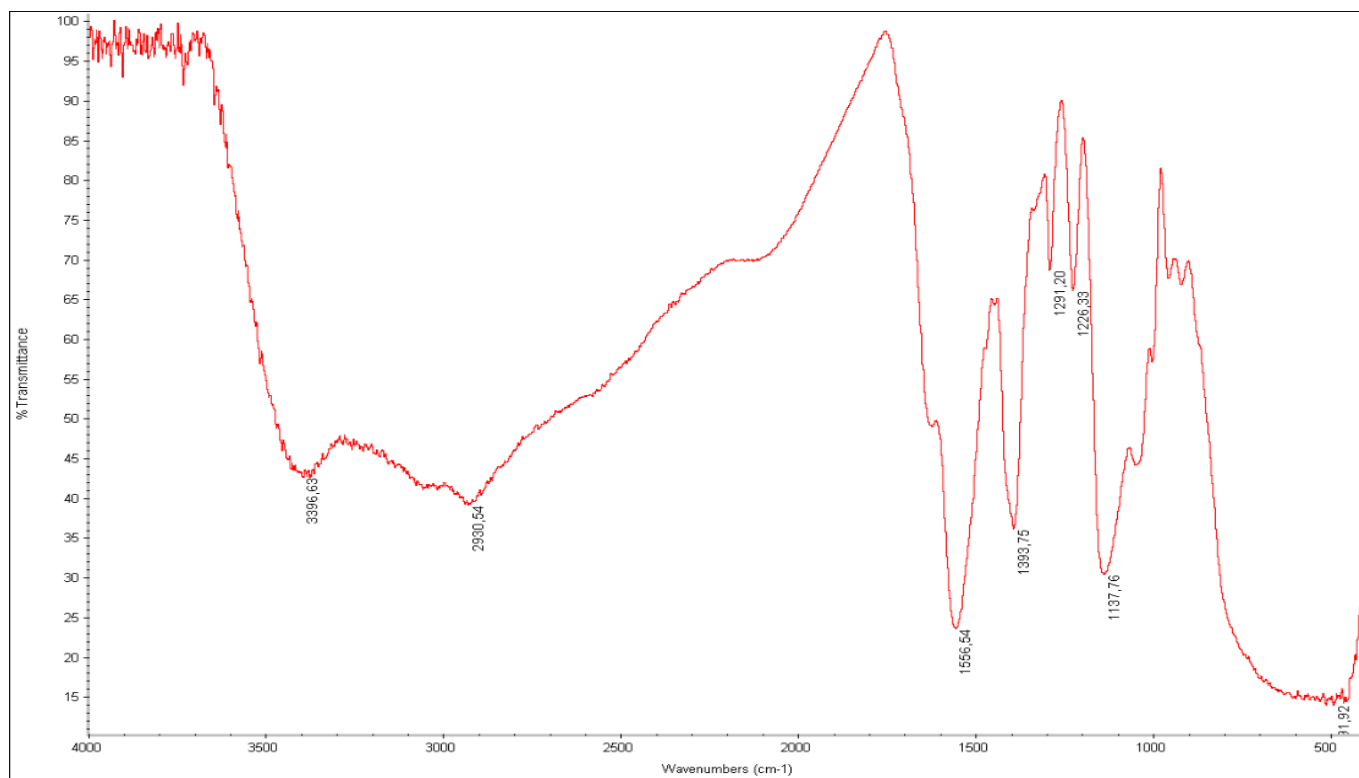


Fig S10b. TGA of P21 @ UiO-66-NH₂ (10); P25 @ UiO-66-NH₂ (11); P100 @ UiO-66-NH₂ (12) composites

Study of structure

Table 4. Particle size for P21 @ UiO-66 (7); P25 @ UiO-66 (8); P100 @ UiO-66 (9); P21 @ UiO-66-NH₂ (10); P25 @ UiO-66-NH₂ (11); P100 @ UiO-66-NH₂ (12)

MOF @ TiO ₂	Particle size (nm)
P21 @ UiO-66	1824
P25 @ UiO-66	1431
P100 @ UiO-66	1144
P21 @ UiO-66-NH ₂	1611
P25 @ UiO-66-NH ₂	2171
P100 @ UiO-66-NH ₂	1031

TiO₂ @ MOF composites. Functionalized process**Fig S11.** FT-IR spectrum of functionalized titanium oxide particle

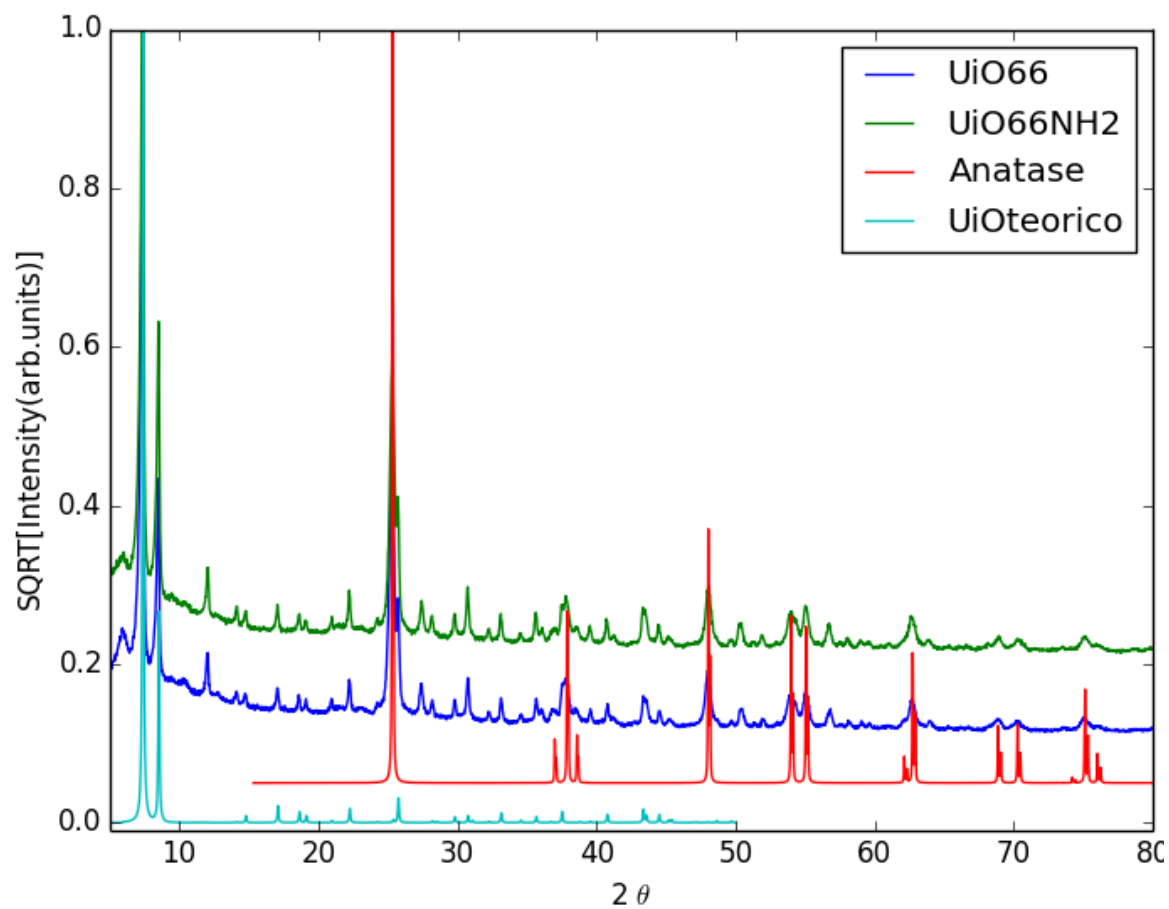


Fig S12. X-Ray powder diffractogram for $\text{TiO}_2\text{-COO @ UiO66}$, and $\text{TiO}_2\text{-COO @ UiO66-NH}_2$ composites

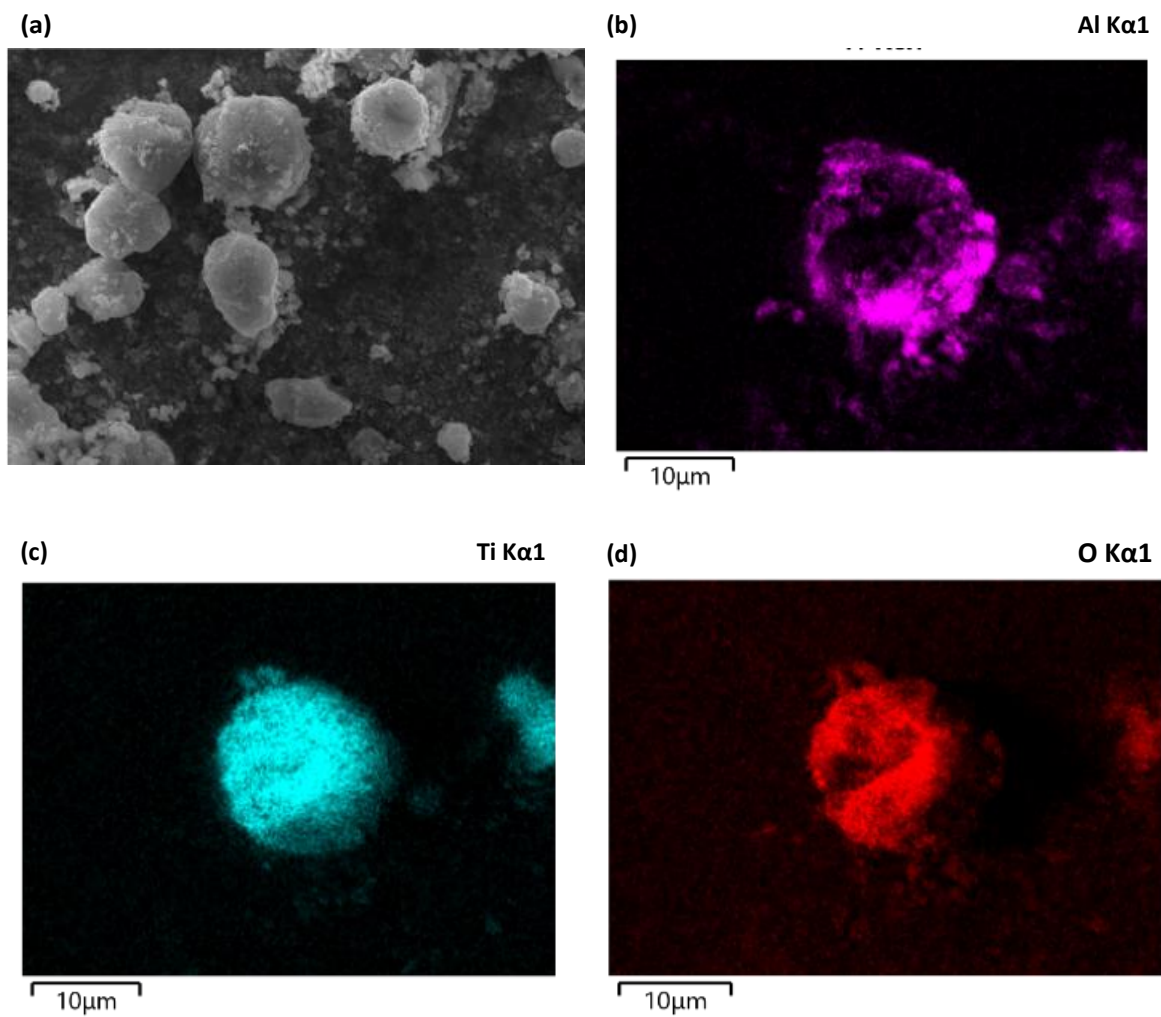
Study of morphology

Fig S14. (a) SEM of **CIM-80 @ TiO₂ (30%) (3)** and elemental mapping of composite (b) aluminium, (c) titanium, (d) oxygen.

ADSOPTION ANALYTES

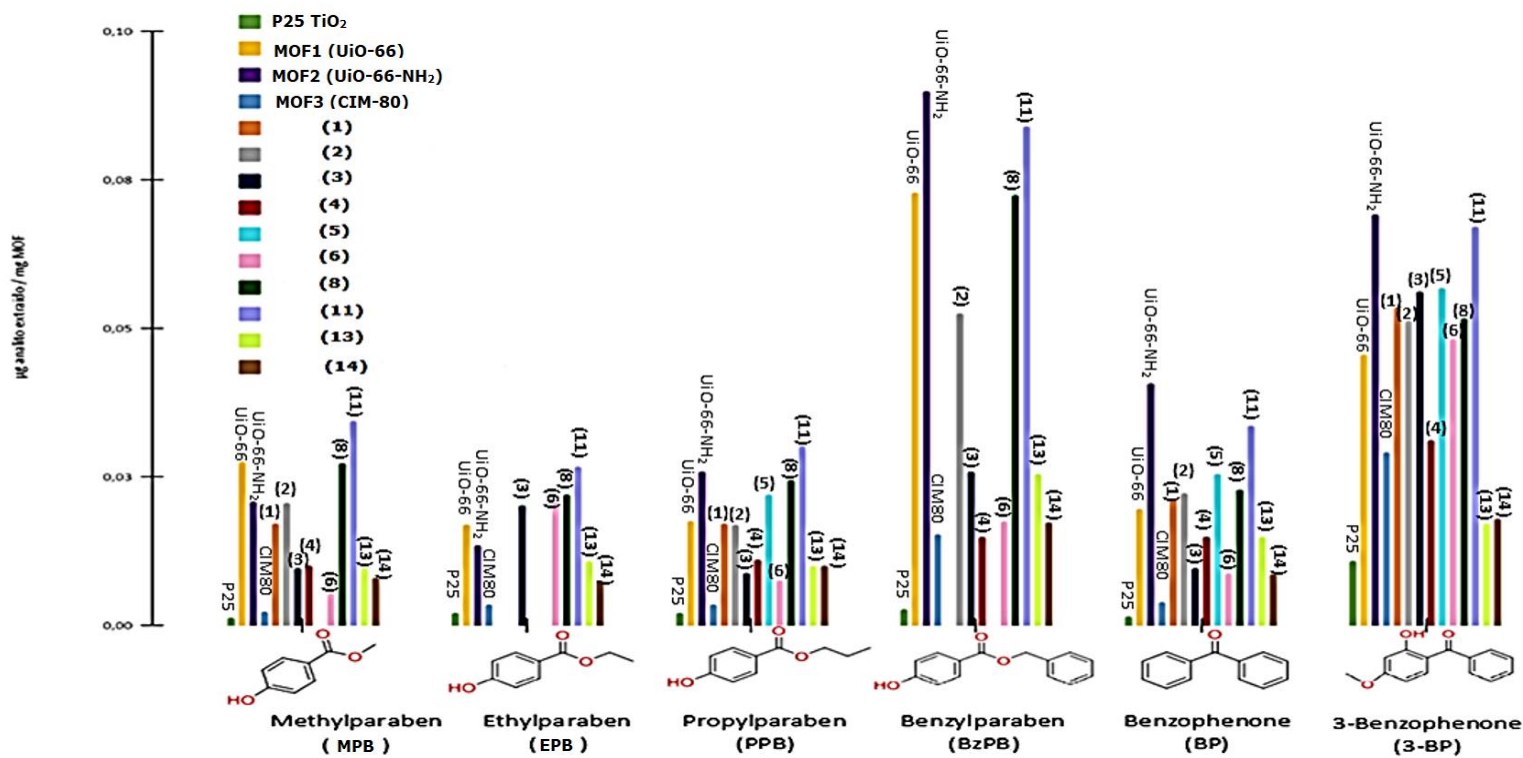


Fig S15. Comparison between the different composites and precursors used in terms of extraction efficiency for each analyte

Table S5. Same of main analytical parameters of chromatographic methods.

Analito	Pendiente	Desviación estándar de la pendiente (Sb)	Ordenada	Desviación estándar de la ordenada (Sa)	R ²	Sx/y	LOD (µg/L)	Intervalo útil (µg/L)	RSD intradía (%)		RSD interdía (%)	
									40 (µg/L)	350 (µg/L)	40 (µg/L)	350 (µg/L)
<i>MPB</i>	1576	12	1736	5935	0,9996	12050	0,75	2,50 - 1000	1,25	0,53	2,27	0,76
<i>EPB</i>	1235	8	761	3932	0,9997	7984	1,50	5,00 - 1000	1,55	0,11	1,64	0,35
<i>PPB</i>	1384	8	-720	3861	0,9998	7839	1,00	3,33 - 1000	0,44	0,69	1,67	0,65
<i>BzPB</i>	921	6	-2083	2756	0,9998	5595	1,50	5,00 - 1000	3,95	1,59	2,44	1,30
<i>PB</i>	1374	11	452	5269	0,9996	10698	2,00	6,67 - 1000	0,79	0,64	1,27	0,90
<i>3-BP</i>	435	5	-1307	2363	0,9993	4798	3,00	10,0 - 1000	10,1	1,33	6,97	1,99